

RECEIVED
LAWRENCE
RADIATION LABORATORY

UCRL-20093

c. 2

NOV 4 1970

LIBRARY AND
DOCUMENTS SECTION

SEARCH FOR POLARIZATION IN ELASTIC e^-p
SCATTERING AT 15 AND 18 GeV

Thomas Mabrey Powell
(Ph. D. Thesis)

August 1970

AEC Contract No. W-7405-eng-48

TWO-WEEK LOAN COPY

*This is a Library Circulating Copy
which may be borrowed for two weeks.
For a personal retention copy, call
Tech. Info. Division, Ext. 5545*

34/2
LAWRENCE RADIATION LABORATORY
UNIVERSITY of CALIFORNIA BERKELEY

UCRL-20093

c. 2

DISCLAIMER

This document was prepared as an account of work sponsored by the United States Government. While this document is believed to contain correct information, neither the United States Government nor any agency thereof, nor the Regents of the University of California, nor any of their employees, makes any warranty, express or implied, or assumes any legal responsibility for the accuracy, completeness, or usefulness of any information, apparatus, product, or process disclosed, or represents that its use would not infringe privately owned rights. Reference herein to any specific commercial product, process, or service by its trade name, trademark, manufacturer, or otherwise, does not necessarily constitute or imply its endorsement, recommendation, or favoring by the United States Government or any agency thereof, or the Regents of the University of California. The views and opinions of authors expressed herein do not necessarily state or reflect those of the United States Government or any agency thereof or the Regents of the University of California.

SEARCH FOR POLARIZATION IN ELASTIC
e⁻p SCATTERING AT 15 and 18 GeV

Contents

Abstract

I.	Introduction.	1
II.	Some Phenomenology and Theory of Elastic Electron-Proton Scattering	3
	A. Polarization in e ⁻ p Scattering in Helicity Representation.	5
	B. Single Photon Exchange.	13
	C. Theoretical Questions Involved in the Search for Two Photon Effects.	20
	1. Deviations from the Rosenbluth Formula.	20
	2. Difference Between Electron-Proton and Positron-Proton Cross Sections.	21
	3. Polarization and Asymmetry Measurements	26
III.	Experimental Apparatus and Procedure.	30
	A. Electron Beam	33
	B. Beam Monitors	37
	C. Counters and Electronics.	37
	D. Spectrometer.	43
	E. Polarized Target.	47
	F. Computer Control.	59
	G. Running Conditions.	60
	H. Fraction of Events from Hydrogen.	62
IV.	Data Analysis.	68
	A. Least Squares Fitting of Polarized Data	68
	B. Test Asymmetries.	72

C.	Two Specific Systematic Checks.	76
D.	Normalization Errors.	77
E.	Selection of Data	79
V.	Results	81
VI.	Discussion of Results	85
	A. Radiative Corrections	85
	B. Other Experiments	88
	Acknowledgments	90
	Appendix I.	92
	References.	97

-v-

SEARCH FOR POLARIZATION IN ELASTIC e^-p SCATTERING AT 15 AND 18 GeV

Thomas Mabrey Powell

Lawrence Radiation Laboratory
University of California
Berkeley, California

August 1970

ABSTRACT

We have measured the asymmetry in the elastic scattering of electrons from a polarized proton target. An interference between the imaginary part of the two-photon-exchange amplitude and the one-photon-exchange amplitude could produce a polarization effect. The results indicate no asymmetry within the experimental accuracy of 1 to 2% at four-momentum transfer squared values of 0.38, 0.59, and 0.98 $(\text{GeV}/c)^2$.

I. INTRODUCTION

The customary reliance on one-photon-exchange calculations in electron-proton scattering makes it important to study those processes which could only arise from higher-order effects. A measurement of non-zero proton polarization in elastic electron-proton scattering would be evidence for a two-photon-exchange amplitude, since the polarization must vanish for pure one-photon exchange. The interference between one-photon-exchange and two-photon exchange amplitudes is expected to be smaller than the one-photon-exchange contribution by an order of α , but it may be enhanced due to the presence of some resonance process.¹

In electron-proton elastic scattering, one-photon exchange leads to the Rosenbluth formula² for the differential cross section. Higher-order effects, which could show up as deviations from the Rosenbluth form, have not been observed so far.³

The interference between the one-photon amplitude and the real part of some two-photon amplitudes can be obtained by comparing electron-proton and positron-proton elastic scattering. These measurements⁴ (after allowing for radiative losses⁵) have shown no evidence of two-photon effects, to an accuracy of about the order α , up to four-momentum transfers squared of 5.0 (GeV/c)^2 .

Information relating to the imaginary part of a different combination of two-photon-exchange amplitudes can be measured by performing a polarization experiment. Two kinds of experiments are possible. One can measure the polarization, P , of the recoiling nucleon in the elastic scattering of unpolarized electrons from an unpolarized proton target. Alternatively (as in the present experiment) one can measure the asymmetry,

A, in the scattering of electrons from a polarized proton target, defined as

$$A = \frac{\sigma(\uparrow) - \sigma(\downarrow)}{\sigma(\uparrow) + \sigma(\downarrow)} = \frac{\epsilon}{|P_T|H_F} \quad (1)$$

where $\sigma(\downarrow), \sigma(\uparrow)$ denote the cross sections on hydrogen polarized parallel and antiparallel to the normal (\hat{n}) to the electron scattering plane. The quantity ϵ is the asymmetry in the raw counts from the polarized target, and the factors P_T, H_F allow for the target proton polarization and the fraction of hydrogen counts present in the data, respectively. We define \hat{n} , as:

$$\hat{n} = \frac{\vec{p}_{in} \times \vec{p}_{out}}{|\vec{p}_{in} \times \vec{p}_{out}|} \quad (2)$$

where \vec{p}_{in} and \vec{p}_{out} are the momenta of the initial and final electron, respectively.

Results of this experiment have already been published⁶ and this dissertation attempts to detail and clarify that publication. In summary, the experiment described herein looked for a two-photon-exchange contribution to the amplitude for elastic electron-proton scattering. None was seen.

II. SOME PHENOMENOLOGY AND THEORY OF ELASTIC ELECTRON-PROTON SCATTERING

Because electrons and protons have spin one-half, as far as the "inessential complications due to spin" are concerned, elastic electron-proton scattering is exactly the same as elastic proton-proton scattering, except that the particles are not identical. Hence one can use such representations as the Wolfenstein formalism⁷ or the helicity representation⁸ almost precisely in the form in which many have applied them to the two-nucleon problem. However, instead of five amplitudes (as in pp scattering) six independent amplitudes enter (in ep scattering) because the particles are not identical, but the analysis proceeds similarly to the two-nucleon case.

The usual Feynman prescription⁹ associates a factor of e (the electron charge) with each photon vertex. Such a single-photon exchange diagram, as shown in Fig. 1a, has a multiplicative factor of e^2 ($=\alpha=1/137$ in units where $\hbar=c=1$). Two-photon-exchange amplitudes, as shown in Fig. 1b, thus have multiplicative factors of $e^4 = \alpha^2$. Hence, searching for two-photon exchange amplitudes entails looking for effects at the one-percent level, because the interference term between single- and double-photon-exchange amplitudes has an extra factor of $\alpha = \frac{1}{137}$ compared to the single-photon-exchange term.

This section will first detail the description of polarizations in the helicity representation and second discuss the theoretical questions which one must consider to understand experimental quantities in terms of the single- and double-photon exchange contributions.

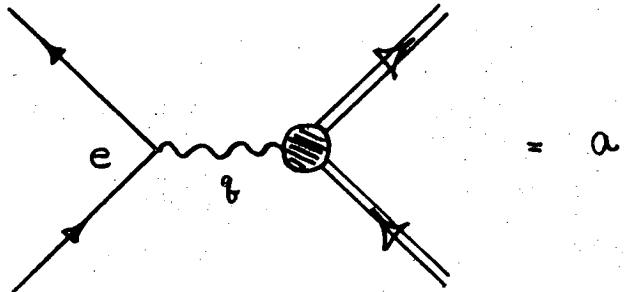


FIG. 1a.

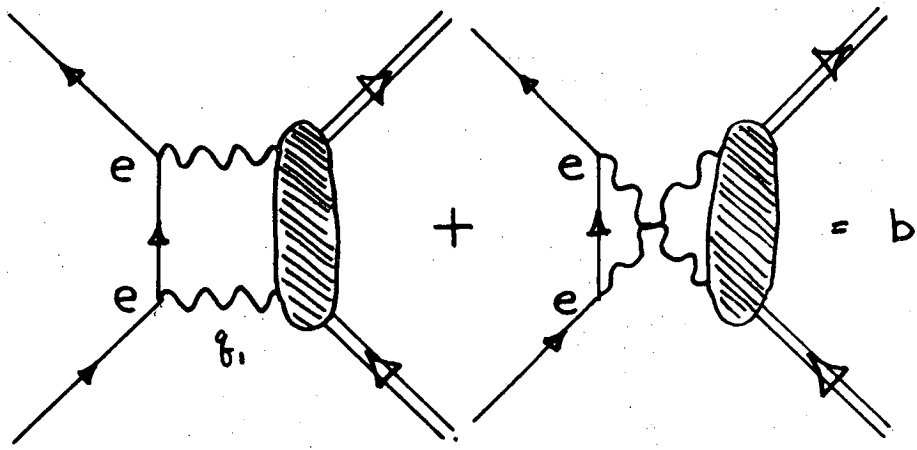


FIG. 1b.

XBL 708-1775

Fig. 1. Single and double photon exchange in e-p scattering.

A. Polarization in e^-p Scattering in Helicity Representation

In the elastic process

$$e^- + p \rightarrow e^- + p \quad (3)$$

we let

$$\lambda_a = \text{initial electron helicity} = \pm \frac{1}{2}$$

$$\lambda_b = \text{initial proton helicity} = \pm \frac{1}{2}$$

$$\lambda_c = \text{final electron helicity} = \pm \frac{1}{2}$$

$$\lambda_d = \text{final proton helicity} = \pm \frac{1}{2} .$$

Jacob and Wick⁸ have demonstrated that one can make a simple partial wave decomposition of the amplitude for scattering from a fixed initial helicity configuration to a fixed final helicity configuration thusly:

$$M_{(\lambda_c \lambda_d)(\lambda_a \lambda_b)} = \frac{1}{2p} \sum (2J+1) d_{\lambda\mu}^J(\theta) \langle \lambda_c \lambda_d | T^J(p) | \lambda_a \lambda_b \rangle \quad (4)$$

where $\lambda = \lambda_a - \lambda_b$ and $\mu = \lambda_c - \lambda_d$; θ is the center-of-mass (c.m.) scattering angle; p the c.m. momentum; and $d_{\lambda\mu}^J(\theta)$ is the matrix representation of dimension $(2J+1)$ of the rotation through angle θ .¹⁰ $\langle \lambda_c \lambda_d | T^J(p) | \lambda_a \lambda_b \rangle$ is the transition matrix amplitude for total angular momentum J . Since $\lambda_a, \dots, \lambda_d$ can each take on two values $= \pm \frac{1}{2}$, $M_{(\lambda_c \lambda_d)(\lambda_a \lambda_b)}$ has sixteen entries. We will use parity and time-reversal invariance to reduce these to six entries.

Helicities change sign under the parity transformation, so if the interaction is invariant under parity,

$$\pi T^J(p) \pi^{-1} = T^J(p) \quad , \quad \text{where}$$

$\pi =$ parity transformation on fixed helicity states,

and

$$\pi |\lambda_a \lambda_b\rangle = |-\lambda_a - \lambda_b\rangle, \text{ then}$$

$$\langle \lambda_c \lambda_d | T^J(p) | \lambda_a \lambda_b \rangle = \langle \lambda_c \lambda_d | \pi^{-1} T^J(p) \pi | \lambda_a \lambda_b \rangle = \langle -\lambda_c - \lambda_d | T^J(p) | -\lambda_a - \lambda_b \rangle \quad (5)$$

Helicities remain unchanged under the time reversal operation, but in taking matrix elements, one must interchange the initial and final states. So if the interaction is time-reversal invariant

$$\langle \lambda_c \lambda_d | T^J(p) | \lambda_a \lambda_b \rangle = \langle \lambda_a \lambda_b | T^J(p) | \lambda_c \lambda_d \rangle. \quad (6)$$

We finally need some properties of the d function,¹⁰ namely,

$$d_{\lambda\mu}^J(\theta) = (-1)^{\lambda-\mu} d_{\mu\lambda}^J(\theta) = (-1)^{\lambda-\mu} d_{-\lambda-\mu}^J(\theta) \quad (7)$$

Now we choose a definite set of helicity basis states.

$$\begin{aligned} \text{Specifically, } |\xi_1\rangle &= |++\rangle \\ |\xi_2\rangle &= |+-\rangle \\ |\xi_3\rangle &= |-+\rangle \\ |\xi_4\rangle &= |--\rangle \end{aligned} \quad (8)$$

The first index (+ or -) refers to the electron's helicity, $h(e^-)$. The second index (+ or -) refers to the proton's helicity, $h(p)$.

We next write the full matrix, M.

$$M = \begin{pmatrix} M_{11} & M_{12} & M_{13} & M_{14} \\ M_{21} & M_{22} & M_{23} & M_{24} \\ M_{31} & M_{32} & M_{33} & M_{34} \\ M_{41} & M_{42} & M_{43} & M_{44} \end{pmatrix} \quad (9)$$

in terms of our choice of basis states.

But

$$\begin{aligned}
 M_{11} &= \frac{1}{2p} \sum_J d_{00}^J(\theta) \langle ++ | T^J(p) | ++ \rangle (2J+1) \\
 &= \frac{1}{2p} \sum_J d_{00}^J(\theta) \langle -- | T^J(p) | -- \rangle (2J+1) \\
 &= M_{44}
 \end{aligned}$$

where we have used the invariance under parity (Eq. (5)) to get the second identity. Further use of parity conservation and properties of the d functions (Eq. (7)) enable one to conclude that

$$M_{14} = M_{41}$$

$$M_{12} = -M_{43}$$

$$M_{13} = -M_{42}$$

$$M_{21} = -M_{34}$$

$$M_{22} = M_{33}$$

$$M_{23} = M_{32}$$

$$M_{24} = -M_{31}$$

Further still,

$$\begin{aligned}
 M_{12} &= \frac{1}{2p} \sum_J d_{10}^J(\theta) \langle ++ | T^J(p) | + - \rangle (2J + 1) \\
 &= \frac{1}{2p} \sum_J d_{10}^J(\theta) \langle + - | T^J(p) | ++ \rangle (2J + 1) \\
 &= \frac{1}{2p} \sum_J (-1) d_{01}^J(\theta) \langle + - | T^J(p) | ++ \rangle (2J + 1) = -M_{21}
 \end{aligned}$$

where we have used time reversal invariance (Eq. (5)) to get the second identity, and the properties of the d functions (Eq. (7)) to get the third identity. We can similarly show that $M_{13} = M_{24}$.

This leaves six independent amplitudes which we choose to be

$$\begin{aligned}
 M_{11} &= \langle ++|M|++ \rangle = \phi_1 \\
 M_{14} &= \langle ++|M|-- \rangle = \phi_2 \\
 M_{22} &= \langle +-|M|+- \rangle = \phi_3 \\
 M_{23} &= \langle +-|M|-+ \rangle = \phi_4 \\
 M_{12} &= \langle ++|M|+- \rangle = \phi_5 \\
 M_{13} &= \langle ++|M|-+ \rangle = \phi_6
 \end{aligned} \tag{10}$$

The M matrix is explicitly

$$M = \begin{pmatrix} \phi_1 & \phi_5 & \phi_6 & \phi_2 \\ -\phi_5 & \phi_3 & \phi_4 & \phi_6 \\ -\phi_6 & \phi_4 & \phi_3 & \phi_5 \\ \phi_2 & -\phi_6 & -\phi_5 & \phi_1 \end{pmatrix} \tag{11}$$

One sees that ϕ_1 and ϕ_3 are amplitudes which involve no helicity flips for either particle; ϕ_2 and ϕ_4 involve helicity flips for both particles; while ϕ_5 and ϕ_6 involve an helicity flip for one of the particles.

The density matrix formalism is very well explained elsewhere,¹¹ and we only quote results necessary for our purposes.

M is our transition operator, a matrix in spin space. The density matrix for the final state, ρ_f , is related to the density matrix for the initial state, ρ_i .

$$\rho_f = M \rho_i M^\dagger . \quad (12)$$

For convenience, we "normalize" the initial state density matrix by demanding that $\text{Tr } \rho_i = 1$.

We define the final state scattered intensity (which is in fact the differential cross section) by

$$I = \text{Tr } \rho_f = \text{Tr } M \rho_i M^\dagger \quad (13)$$

Using the helicity representation, we construct the initial-state density matrix out of the direct product of the initial state density matrices for each of the particles.

$$\rho_i = \rho_i^{(e)} \otimes \rho_i^{(p)} . \quad (14)$$

We must remember that our choice of the helicity basis has led us to quantize the spin of each particle along its direction of motion. Also the use of the $d_{\lambda\mu}^J(\theta)$ functions has implied that the normal to the scattering plane is along the \hat{y} direction.¹⁰ Explicitly, we calculate the initial-state density matrices for an unpolarized electron state ($\rho_i^{(e)}$) and a proton state polarized to an extent P_T in the \hat{y} direction ($\rho_i^{(p)}$).

$$\rho_i^{(e)} = \frac{1}{2} \mathbb{1} = \frac{1}{2} \begin{pmatrix} 1 & 0 \\ 0 & 1 \end{pmatrix} \quad (15)$$

$$\rho_i^{(p)} = \frac{1}{2} (\mathbb{1} + P_T \sigma_y) = \frac{1}{2} \begin{pmatrix} 1 & -iP_T \\ i P_T & 1 \end{pmatrix} \quad (16)$$

so

$$\rho_i = \rho_i^{(e)} \otimes \rho_i^{(p)} = \frac{1}{4} \begin{pmatrix} 1 & -i P_T & 0 & 0 \\ i P_T & 1 & 0 & 0 \\ 0 & 0 & 1 & -i P_T \\ 0 & 0 & i P_T & 1 \end{pmatrix} \quad (17)$$

where the same basis as used for M is used to represent ρ_i .

We use these results to calculate the final-state scattered intensities.

Case I: unpolarized cross section. Here

$$\rho_i = \frac{1}{4} \mathbb{1}$$

so

$$\begin{aligned} I_0 &= \text{Tr } \rho_f = \frac{1}{4} \text{Tr}(MM^\dagger) \\ &= \frac{1}{2} \left(|\phi_1|^2 + |\phi_2|^2 + |\phi_3|^2 + |\phi_4|^2 + 2|\phi_5|^2 + 2|\phi_6|^2 \right) \end{aligned} \quad (18)$$

Case II: scattering unpolarized electrons from a polarized proton target.

Here

ρ_i is given by Eq. (17) and

$$I = \text{Tr } M \rho_i M^\dagger = I_0 (1 + P_T A) \quad (19)$$

where

$$A = \frac{1}{I_0} \text{Im}(\phi_1 \phi_5^* - \phi_2 \phi_6^* + \phi_3 \phi_5^* + \phi_4 \phi_6^*) \quad (20)$$

The asymmetry A is the quantity this experiment measures; namely, we polarize the proton target in the $+\hat{y}$ direction (\uparrow) and measure $I(\uparrow)$, then we polarize the proton target in the $-\hat{y}$ direction and measure $I(\downarrow)$.

Finally,

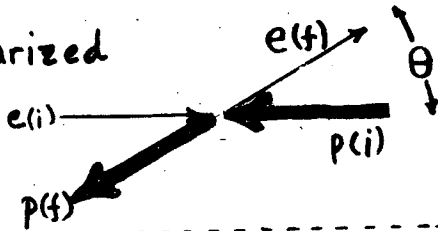
$$A = \frac{1}{P_T} \frac{I(\uparrow) - I(\downarrow)}{I(\uparrow) + I(\downarrow)}. \quad (21)$$

Conventionally, one calls the polarization parameter, P , the polarization of one of the final particles when both initial particles are unpolarized. In e^-p elastic scattering, if one lets unpolarized electrons impinge on unpolarized protons and measures the polarization of the final recoiling proton he measures P . This is simply the time reversed situation from the present experiment. A graphic illustration of this statement is given Fig. 2. If the electromagnetic interaction, through which the electron and proton interact, is time-reversal invariant, $A = P$.

INITIALLY

$e(i)$ unpolarized

①

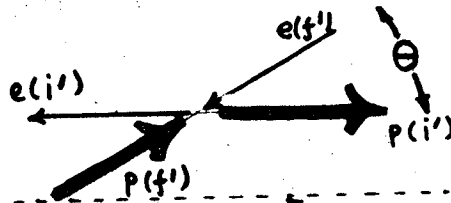


$p(i)$ has polarization P_T , out of plane of paper

⊙

under time-reversal, momenta and spins are reversed

②

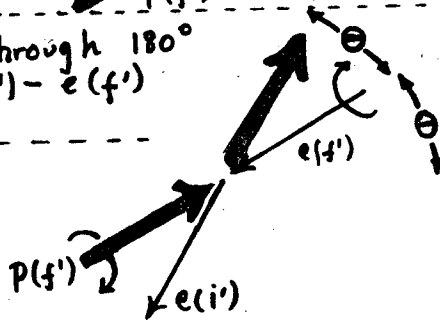


P_T into plane of paper

⊗

rotation through 180° about $p(f') - e(f')$ axis

③

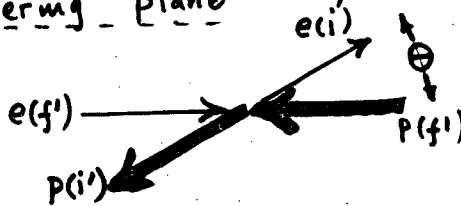


P_T out of plane of paper

⊙

rotation through angle $180^\circ - \theta$ about normal to the scattering plane

④



P_T out of plane of paper

⊙

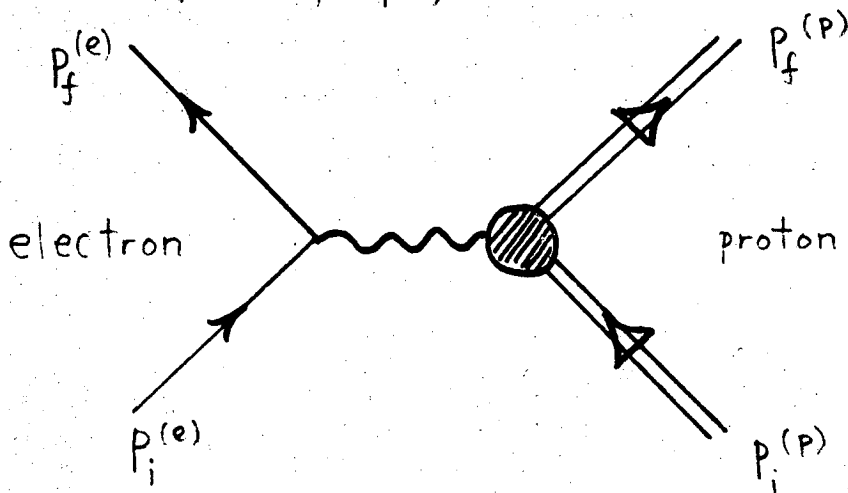
XBL 708-1776

Fig. 2. Rotational Invariance and Time Reversal Invariance imply $A = P$.

B. Single Photon Exchange

Up to the present date, there has been no need to include two photon exchange terms in the description of elastic e^-p scattering.^{3,4,12} The predictions of the Feynman prescription for calculating the single-photon-exchange diagram in Fig. 1a are borne out by experiment.¹³ We note that due to the charge density and anomalous magnetic moment of the proton, two arbitrary functions, called form factors, correct the Dirac term for the proton current. If the proton were purely a Dirac particle, like the electron, these functions would be constants, equal to unity. Using the metric and normalizations of Ref. 9, we write the e^-p scattering amplitude as¹⁴

$$M_{fi} = \frac{1}{\sqrt{(16 E_f^{(p)} E_i^{(p)} E_f^{(e)} E_i^{(e)})}} \left(J_\mu^{(p)} \frac{1}{q^2} j_\mu^{(e)} \right) (2\pi)^4 \delta(p_f^{(p)} - p_i^{(p)} + p_f^{(e)} - p_i^{(e)}) \quad (22)$$



$$q^2 = (p_f^{(e)} - p_i^{(e)})^2 = (p_f^{(p)} - p_i^{(p)})^2 = (4\text{-momentum-transfer})^2$$

q^2 is positive in the physical region for $e-p$ scattering.

The lines of the above diagram are labeled by their respective 4-momenta, $p_f^{(e)}, \dots, p_i^{(p)}$; $E_f^{(e)}, \dots, E_i^{(p)}$ are the time components of these 4-vectors, respectively. $J_\mu^{(p)}$, the proton current is

$$J_\mu^{(p)} = e \left\langle \bar{u}(p_f^{(p)}) \left| \gamma_\mu F_1(q^2) + i \sigma_{\mu\nu} q_\nu \frac{\chi_p}{2M_p} F_2(q^2) \right| u(p_i^{(p)}) \right\rangle \quad (23)$$

F_1 and F_2 are the arbitrary functions, depending only on q^2 , which are called the Dirac form factors.¹⁵ They are normalized so that $F_1(0) = F_2(0) = 1$. $\frac{1}{q^2}$ = photon propagator. $j_\mu^{(e)}$, the electron current, $= e \left\langle \bar{u}(p_f^{(e)}) \left| \gamma_\mu \right| u(p_i^{(e)}) \right\rangle$. χ_p = anomalous portion of the proton's magnetic moment (in nuclear magnetons) = 2.79 - 1, while M_p = mass of the proton.

That there are only two such arbitrary functions, and that the proton current has precisely the above form is a direct consequence of the very general requirements of Lorentz invariance, parity conservation in EM interactions, the fact that free protons and electrons satisfy the free particle Dirac equation, and current conservation.¹⁴

From this explicit form for the amplitude, one can tediously calculate a cross-section. In the LAB frame where the target proton is at rest, if one neglects the electron mass, the differential cross-section takes the form

$$\left(\frac{d\sigma}{d\Omega} \right)_{\text{LAB}} = \left(\frac{d\sigma}{d\Omega} \right)_{\text{NS}} \left[\frac{G_E^2 + \tau G_M^2}{1 + \tau} + 2\tau G_M^2 \tan^2 \frac{\theta}{2} \right]. \quad (24)$$

G_E and G_M are defined in reference 15. While $\tau = \frac{q^2}{4M_p^2}$; θ is the the laboratory scattering angle and $\left(\frac{d\sigma}{d\Omega} \right)_{\text{NS}}$ is called the Mott-cross section,

$$\left(\frac{d\sigma}{d\Omega}\right)_{NS} = \left(\frac{\alpha}{2E_0}\right)^2 \frac{\cos^2 \frac{\theta}{2}}{\sin^4 \frac{\theta}{2}} \cdot \frac{1}{1 + \frac{2E_0}{M_p} \sin^2 \frac{\theta}{2}}$$

E_0 is the incident electron energy in the LAB frame. Equation (24) is known as the Rosenbluth formula.² We note three things about the Rosenbluth formula: first,

$$\left(\frac{d\sigma}{d\Omega}\right)_{LAB} = \left(\frac{d\sigma}{d\Omega}\right)_{NS} \left[A(q^2) + B(q^2) \tan^2 \frac{\theta}{2} \right]. \quad (25)$$

This form is only a consequence of the single-photon-exchange assumption;¹⁶ second, the relative sign of G_E and G_M cannot be determined from the Rosenbluth cross-section, because only the squares of G_E and G_M enter; third, all of the present data (except for some recent SLAC data at the highest energies and q^2 values¹³) can be fit with the empirical form,

$$G_E(q^2) = \frac{G_M(q^2)}{2.79} = \frac{G_M(q^2)}{1 + \kappa_p} = \frac{1}{\left(1 + \frac{q^2}{0.71}\right)^2} \cdot \quad (26)$$

q^2 in $(\text{GeV}/c)^2$

This is called the "dipole fit," and no theoretical reason exists for its excellent agreement with experiment over three orders of magnitude.

After this general background on the single-photon-exchange approximation, we wish to show that very general considerations demand that the polarization (or the asymmetry, A , which the present experiment measured) must vanish, in single-photon-exchange approximation.

We start from the unitarity condition on the S-matrix, $SS^\dagger = \mathbb{1}$. One can always write $S = \mathbb{1} + iT$ (where $T \propto$ our M matrix). Then, $SS^\dagger = (\mathbb{1} + iT) \cdot (\mathbb{1} - iT^\dagger) = \mathbb{1} + i(T - T^\dagger) + TT^\dagger$. We may neglect the term TT^\dagger in this expression, if we insist upon single-photon-exchange approximation. The

TT^\dagger term has an added factor of $e^2 = \alpha = \frac{1}{137}$, when compared with either the T or T^\dagger term. In this approximation, then $T = T^\dagger$, or writing out matrix elements explicitly

$$T_{fi} = T_{if}^* \quad (27)$$

We next assert (and relegate proof to Appendix I) that the single-photon-exchange amplitude is explicitly time-reversal invariant. This assertion is decidedly nontrivial. Even though the full electromagnetic interaction between electron and proton may be time-reversal invariant, each term need not have the same symmetry properties as the full sum. The reason the assertion is true is the fact that current conservation makes the form factor which multiplies the T -violating term vanish.¹⁷

We remember that the time reversal operator reverses all momenta and spins and interchanges initial and final states (because it is anti-unitary). Hence under this operation (and the assumed T invariance),

$$(T_{if})^* = (T_{f^t i^t})^* \quad (28)$$

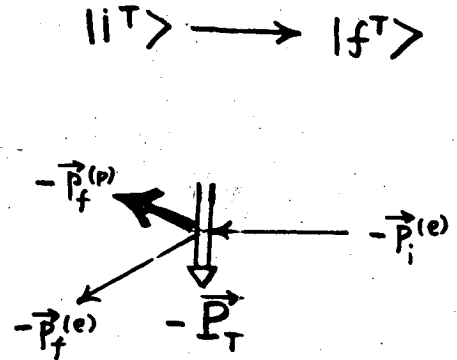
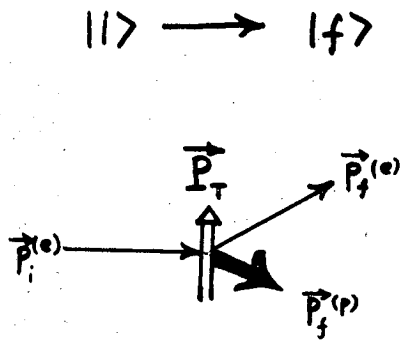
where the states $|f^t\rangle$ and $|i^t\rangle$ are the states $|f\rangle$ and $|i\rangle$ with spins and momenta reversed.

Cross sections $\propto |T\text{-matrix elements}|^2$. Thus, using Eqs. (27) and (28)

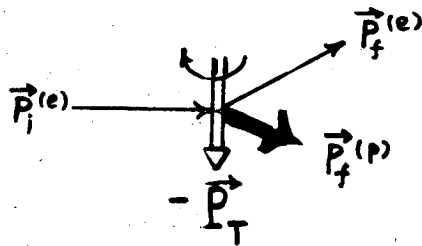
$$\sigma_{fi} = K |T_{fi}|^2 = K |T_{f^t i^t}|^2 = \sigma_{f^t i^t} \quad (29)$$

where K is simply a constant of proportionality, depending on kinematic factors, etc.

Since $|T_{f^t i^t}|^2$ is invariant under rotations, we can relate σ_{fi} to $\sigma_{f^t i^t}$. Figure 3 shows how a rotation about the normal to the scattering plane sets the momenta of $|f^t\rangle$ and $|i^t\rangle$ equal to the momenta of $|f\rangle$



perform a rotation of 180° about the normal to the scattering plane



Above is the process $(|i\rangle \rightarrow |f\rangle)$ except the target polarization is reversed.

XBL 708-1774

Fig. 3.

and $|i\rangle$. Note, especially that the spins of $|f^t\rangle$ and $|i^t\rangle$ remain unchanged if these spins are normal to the plane of scattering. This graphic proof permits us to say that $\sigma_{fi} = \sigma_{f^t i^t}$, where now $|f^t\rangle$ and $|i^t\rangle$ are the same states as $|f\rangle$ and $|i\rangle$ except with spins reversed.

Finally, we sum over all final-state spins (both electron and proton spins) in $|f\rangle$ and $|f^t\rangle$ because this experiment observes no spins in the final state. Because the order of summation is irrelevant,

$$\sum_f = \sum_{f^t},$$

hence as long as both spin states for each particle are summed over $|f\rangle = |f^t\rangle$. Also we sum over the initial electron spins in both $|i^t\rangle$ and $|i\rangle$, because we observe no initial electron spins. The final result is

$$\sum_f \sigma_{fi} = \sum_{f^t} \sigma_{f^t i^t}$$

where the spin of only the proton in $|i^t\rangle$ is opposite to the spin of only the proton in $|i\rangle$. We note this proof is true only for the target proton polarized normal to the plane of scattering. Of course, for a target polarized in the plane of scattering, there is no asymmetry because of parity conservation.

This exposition demonstrates that if one measures a number for the cross section with the target proton polarized in one direction normal to the scattering plane, then reverses the direction of polarization he will measure exactly the same number for that cross section.

The proof hinges on four assumptions: unitarity, rotational

invariance, current conservation (or time-reversal invariance), and single-photon-exchange approximation. One need not belabor the fact that if this experiment measured a non-zero asymmetry surely one would say that the single-photon-exchange approximation had broken down.

C. Theoretical Questions Involved in the Search for Two-Photon Effects

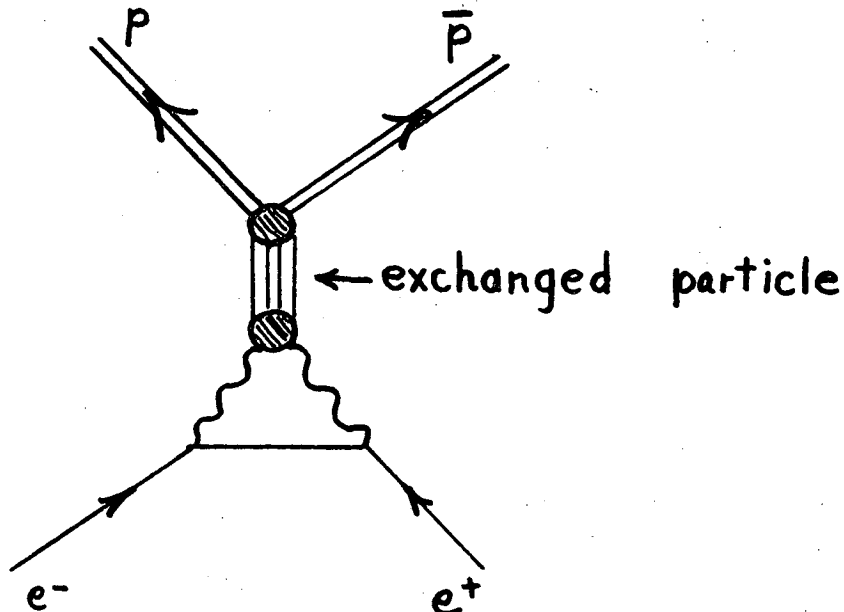
1. Deviations from the Rosenbluth Formula

The most common way to look for two-photon effects is to look for deviations from the Rosenbluth form, Eq. (25). Explicitly, the experimenter measures $\left(\frac{d\sigma}{d\Omega}\right)_{\text{LAB}}$ at fixed q^2 , but varies the LAB scattering angle, θ . (He must then vary the incident electron energy, E_0 , because $q^2 \approx -[4E_0^2 \sin^2\theta/2]/[1 + 2E_0/M \cdot \sin^2\theta/2]$). He then plots

$$\frac{1}{\tan^2 \frac{\theta}{2}} \frac{\left(\frac{d\sigma}{d\Omega}\right)_{\text{LAB}}}{\left(\frac{d\sigma}{d\Omega}\right)_{\text{NS}}} \quad \text{vs.} \quad \cot^2 \frac{\theta}{2} .$$

This plot must be a straight line if Eq. (25) holds.

Unfortunately, such a plot seems to be most sensitive to deviations at quite small laboratory angles,¹⁶ where experiments of sufficient precision have not been performed. Gourdin, and Griffy and Schiff,¹⁶ have discovered the form that one expects the two-photon exchange terms will take, by looking at exchanges in the crossed channel, $e^+e^- \rightarrow p\bar{p}$.



Indeed, these authors show

$$\frac{1}{\tan^2 \frac{\theta}{2}} \frac{\left(\frac{d\sigma}{d\Omega}\right)_{\text{LAB}}}{\left(\frac{d\sigma}{d\Omega}\right)_{\text{NS}}} = \sum_{j=0} c_j(q^2) \left[1 + \frac{\cot^2 \frac{\theta}{2}}{1 - q^2/4M^2} \right]^{j/2}$$

(a series expansion in $[1 + (\cot^2 \frac{\theta}{2})/(1 - q^2/4M^2)]^{1/2}$). Thus to enhance a small two-photon effect one must choose $\theta \approx 0^\circ$ to make $\cot^2 \frac{\theta}{2}$ very large. Such effects have not been seen. These authors further explain that if J^{PC} of the only exchanged particle is 0^{-+} (like a π^0 !) then a two-photon term can lead to no deviations from Eq. (25).

2. Difference between Electron-Proton and Positron-Proton Cross Sections

Referring back to Fig. 1, where the single-photon-exchange amplitude is called a , and the sum of two-photon-exchange amplitudes is called b , we see that $a \propto e$, $b \propto e^2$, where e is the lepton charge. Thus, for positron-proton scattering

$$\sigma(e^+) \propto |a + b|^2 \quad (30)$$

while for electron-proton scattering,

$$\sigma(e^-) \propto |a - b|^2. \quad (31)$$

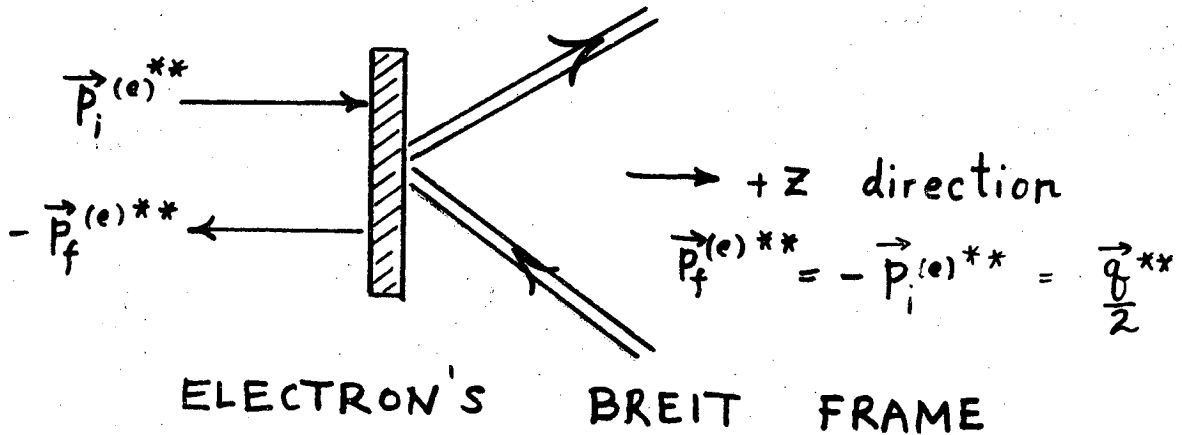
Thus

$$R \equiv \frac{\sigma(e^+) - \sigma(e^-)}{\sigma(e^+) + \sigma(e^-)} \approx 2 \operatorname{Re} \frac{b^* a}{|a|^2} \quad (32)$$

where we have kept only lowest order terms in α . These formulas actually apply only in the case of spinless particles and must be modified to take into account all the helicity amplitudes which may enter into a given process, as in Eq. (18). However, the sense of the demonstration is clear: a non-zero measurement of R is unequivocal proof of a two-photon exchange contribution.

Because there are only two form factors in the single-photon-exchange amplitude, there must be only two independent helicity amplitudes occurring in the single-photon-exchange term. It is easiest to see which two amplitudes (out of the possible six) are independent and non-zero in the high-energy limit.

At high energies the helicity of the electron is unchanged. This is most easily seen by calculating the electron current in the Breit frame of the electron¹⁸ (see below). In the electron's Breit frame $\vec{p}_i^{(e)} = -\vec{p}_f^{(e)}$, hence the name "brick-wall frame." We denote quantities in this frame by two asterisks, **.



The electron current is,

$$j_\mu^{(e)} = e \langle \bar{u}(p_f^{(e)}) | \gamma_\mu | u(p_i^{(e)}) \rangle \quad (33)$$

We use an explicit representation of the γ -matrices and properties of the solutions of the free-particle Dirac equation (in this representation),⁹ namely

$$\vec{\gamma} = \begin{pmatrix} 0 & \vec{\sigma} \\ -\vec{\sigma} & 0 \end{pmatrix}, \quad \gamma_0 = \beta = \begin{pmatrix} \mathbb{1} & 0 \\ 0 & -\mathbb{1} \end{pmatrix}$$

and then

$$u(p) = \sqrt{\frac{E_p + m_e}{2m_e}} \begin{pmatrix} \chi \\ \frac{\vec{\sigma} \cdot \vec{p}}{E_p + m_e} \chi \end{pmatrix}, \quad E_p^2 = \vec{p}^2 + m_e^2$$

where the three components of $\vec{\sigma}$ are the three 2×2 Pauli spin matrices

and $\mathbb{1}$ is the 2×2 unit matrix. $u(p)$ is a 4-component Dirac spinor,

while χ is a two component Pauli spinor. $\chi^\dagger \chi$ is normalized to 1, while

$\bar{u}u = 1$. In the Breit frame $\vec{p}_i^{**} = -\vec{p}_f^{**}$; thus $q^{**} = 4\text{-vector} =$

$$(\vec{p}_f^{**} - \vec{p}_i^{**}) = (0, -2\vec{p}_i^{**}) = (0, 2\vec{p}_f^{**}) = q^{**}. \quad (34)$$

We make explicit use of the identity $(\vec{\sigma} \cdot \vec{A})(\vec{\sigma} \cdot \vec{B}) = \vec{A} \cdot \vec{B} + i\vec{\sigma} \cdot (\vec{A} \times \vec{B})$

which is valid for any vectors \vec{A} and \vec{B} . The result of this evaluation is

that

$$j_0^{**} = e \chi_f^* \chi_i \quad (35)$$

$$\vec{j}^{**} = \frac{e}{i} \chi_f^* \left[\vec{\sigma} \times \frac{\vec{q}^{**}}{2m_e} \right] \chi_i \quad (36)$$

Since $q^2 = -q_0^{**2} + \vec{q}^{**2} = +q^{**2}$, j^{**} is of order

$$\frac{q^2}{4m_e^2},$$

while j_0^{**} is of order 1. Since $m_e \approx 5 \times 10^{-4}$ GeV, an high energy

experiment away from the forward direction will have

$$\frac{q^2}{4m_e^2} \gg 1.$$

We thus neglect j_0^{**} . Further, if we choose \vec{p}_i^{**} in the z-direction,

$j_z^{**} = 0$. This leaves only $j_x^{**} \propto \sigma_y$, $j_y^{**} \propto \sigma_x$. This shows that

the virtual photon is purely transverse in this frame.

If one starts with an initial electron of + helicity (spin in the +z direction, parallel to $\vec{p}_i^{(e)**}$), then $\chi_i = \begin{pmatrix} a \\ 0 \end{pmatrix}$. Because the diagonal elements of $\sigma_x = \begin{pmatrix} 0 & 1 \\ 1 & 0 \end{pmatrix}$ and $\sigma_y = \begin{pmatrix} 0 & -i \\ i & 0 \end{pmatrix}$ vanish, j_x^{**} and j_y^{**} vanish unless χ_f is of the form $\chi_f = \begin{pmatrix} 0 \\ b \end{pmatrix}$, i.e. the final electron has its spin in the -z direction. This proves helicity conservation for the electron because the spin of the final electron must be parallel to $\vec{p}_f^{(e)**}$.

We can also use the fact that for the single photon exchange amplitude alone, an helicity amplitude ϕ_i , $i = 1, \dots, 6$ can be factored into an electron helicity amplitude and a proton helicity amplitude. This is readily seen from the current-current form of interaction, Eq. (22).

Thus

$$\phi_i = f_i^{(e)}(\lambda_a, \lambda_c) F_i^{(p)}(\lambda_b, \lambda_d) \quad (37)$$

where $f_i^{(e)}$ depends only upon electron helicities and $F_i^{(p)}$ depends only on proton helicities.

Neither helicity conservation nor factorization hold for two-photon-exchange amplitudes. Factorization clearly fails, because to calculate an amplitude (as given by b in Fig. 1) one must do a 4-dimensional loop integral over all values of q_1 , the 4-momentum of one of the exchanged photons. One cannot break up this integral into an electron integral and proton integral. Helicity conservation fails because, within the range of this integration, q_1 may take on values such that $|q_1^2/m_e^2| \ll 1$, then an helicity flip at the single photon vertex becomes more probable than no flip (see Eq. (35), (36)).

We will use symmetry principles along with helicity conservation and the factorization of the amplitude to eliminate all but two of the

six amplitudes, Eq. (10). Immediately, ϕ_2 , ϕ_4 , and ϕ_6 vanish because in each of these amplitudes the electron's helicity changes. To establish another relation we observe that

$$\phi_3 = \langle + - | M | + - \rangle = f_3^{(2)}(+,+) F_3^{(p)}(-, -) .$$

is an invariant to which the 0 components contribute negligibly in the Breit frame as long as $q^2 \gg m_e^2$. Since the hadron current $J_\mu^{(p)}$ is known to be a vector under proper and improper Lorentz transformation, it follows that under the space reflection operation $\vec{J}^{(p)}$ must change sign, or,

$$F_3^{(p)}(-, -) = -F_3^{(p)}(+, +)$$

$$\phi_3 = - f_3^{(e)}(+,+) F_3^{(p)}(+, +) = - \phi_1 .$$

This leaves only ϕ_1 and ϕ_5 as independent helicity amplitudes in single photon exchange.

We can write each helicity amplitude, ϕ_i , as sum of two contributions: the first, a_i , is a single-photon-exchange term; the second, b_i , is a two-photon-exchange term. Thus,

$$\begin{aligned} \phi_1 &= a_1 + b_1 \\ \phi_2 &= b_2 \\ \phi_3 &= - a_1 + b_3 \\ \phi_4 &= b_4 \\ \phi_5 &= a_5 + b_5 \\ \phi_6 &= b_6 \end{aligned} \quad (38)$$

Using Eq. (18), we can write

$$\sigma(e^+) = \frac{1}{2} \left\{ |a_1 + b_1|^2 + |b_2|^2 + |-a_1 + b_3|^2 + |b_4|^2 + 2|a_5 + b_5|^2 + 2|b_6|^2 \right\} (39)$$

while

$$\sigma(e^-) = \frac{1}{2} \left\{ |a_1 - b_1|^2 + |-b_2|^2 + |-a_1 - b_3|^2 + |-b_4|^2 + 2|a_5 - b_5|^2 + 2|-b_6|^2 \right\} \quad (40)$$

$$R = \frac{\sigma(e^+) - \sigma(e^-)}{\sigma(e^+) + \sigma(e^-)} \approx \frac{\text{Re}[(b_1^* - b_3^*)a_1 + 2a_5^* a_5]}{|a_1|^2 + |a_5|^2} \quad (41)$$

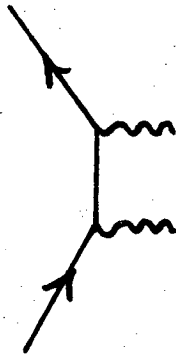
3. Polarization and Asymmetry Measurements

A calculation of a similar nature leads to an expression for A,

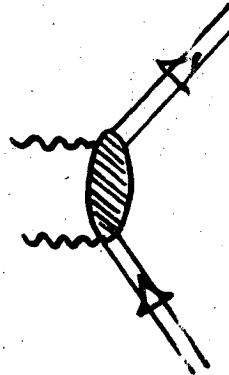
$$A \approx - \frac{\text{Im}[a_5(b_1^* + b_3^*)]}{|a_1|^2 + |a_5|^2} \quad (42)$$

We see that A measures the imaginary parts of amplitudes b_1 and b_3 while, R measures the real parts of amplitudes b_1 , b_3 , and b_5 . It is a commonly held belief that "R measures the real part of two photon exchange amplitudes, while A measures the imaginary part of two photon exchange amplitudes." We see that the situation is considerably more delicate than this simple statement. Let us pose a hypothetical case: if b_1 , b_3 , and b_5 vanish, but b_2 , b_4 , and b_6 are non-zero, then $A=R=0$; yet the b_2 , b_4 , and b_6 amplitudes might be sizeable. Indeed, if b_1 , b_3 , and b_5 were pure imaginary, then the expression for the cross-section, Eq. (40), would have correction terms of order $|b_1|^2$ i.e. only of order α^4 . All terms like $\text{Re}(a_1 b_1^*)$ would vanish because a_1 and a_5 are known to be purely real (see Appendix I). There is considerable belief that the two-photon-exchange amplitudes should be primarily imaginary.¹⁹ This is because the two-photon term is related to virtual

Compton Scattering.



virtual Compton scattering



The intermediate state in the virtual Compton diagram could be the nucleon, $\Delta(1238)$, $N^*(1512)$, etc. The real Compton cross-section is dominated by a huge resonance at ≈ 300 MeV (incident γ LAB energy) corresponding to the $\Delta(1238)$. The belief is that the virtual process is dominated by this (or other) resonances. The resonance amplitude, a Breit-Wigner form,

$$T(E) = \frac{\Gamma/2}{(E_R - E) - i \Gamma/2}$$

is pure imaginary at the resonance energy, $E = E_R$. Hence the claim that the virtual Compton scattering is close to being pure imaginary.

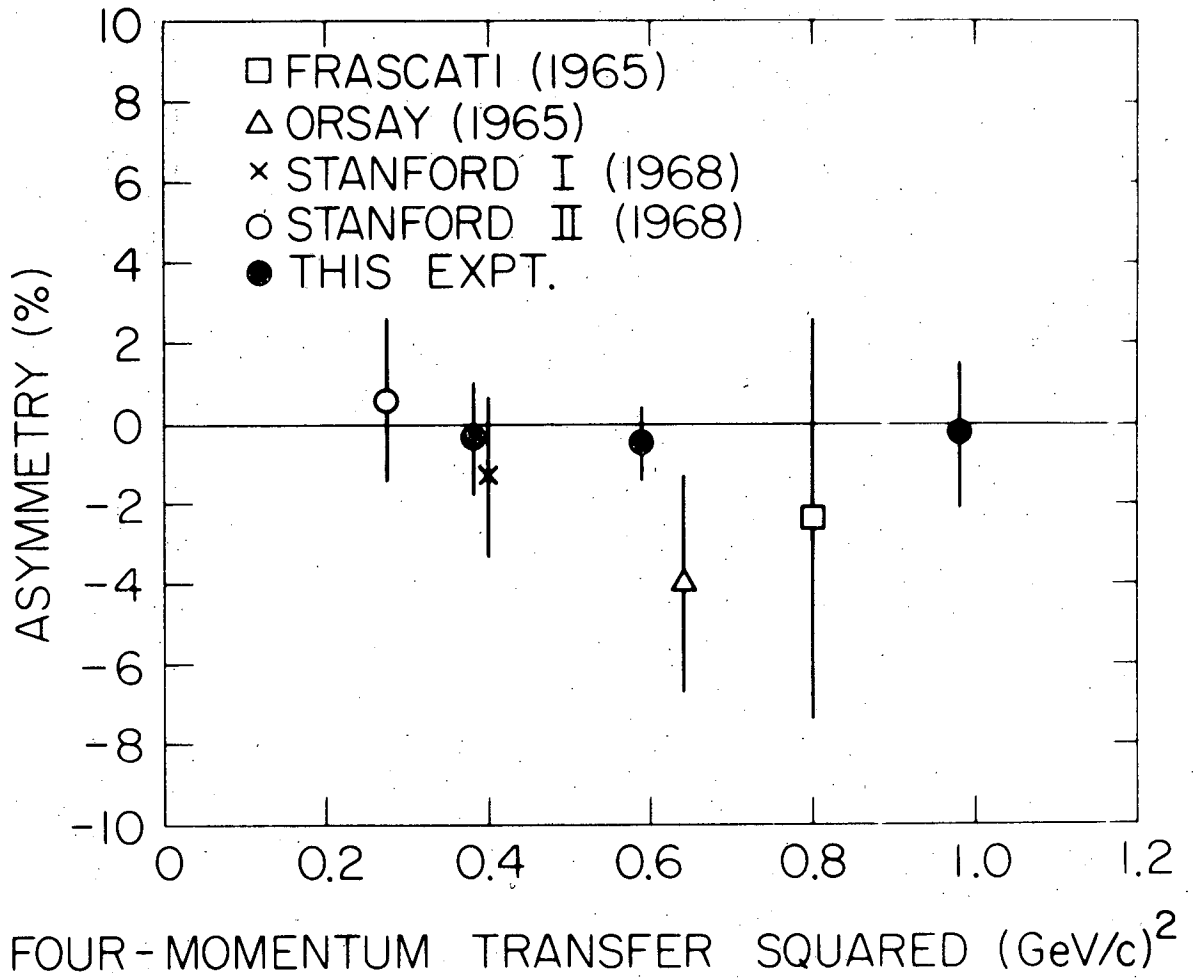
These intuitive ideas and the analysis leading up to Eqs. (41) and (42) lead one to the conclusion that looking for an asymmetry, A (or polarization, P), has the best chance of seeing a two-photon effect, because measurements of an electron-positron difference, R, or deviations from the Rosenbluth form seek a real part of two-photon terms, while the two-photon contribution is probably dominated by its imaginary part.

Three theoretical calculations of P (and thus A) exist.²⁰ Their predictions are that P is never larger than 1/2%. One should note that

only one of these predictions (Arafune and Shimizu) extends above 1 GeV incident electron energy, while the experiment here reported was performed at 15 and 18 GeV.

Four previous measurements of P have been reported.¹² All four measurements were performed at or below 1 GeV incident electron energy, but at similar values of q^2 , $(0.3(\text{GeV}/c)^2 \leq 1.0(\text{GeV}/c)^2)$. These data, along with data from the present experiment are shown in Fig. 4. All of these polarizations are consistent with zero.

One might ask if some other spin correlation measurement could give a combination of amplitudes which would be particularly sensitive to two-photon exchange. Three Russian authors²¹ have derived a general formalism for spin correlation experiments in which the target proton is polarized in the plane of scattering and either, one, the incident electron beam is polarized in the plane of scattering, or, two, the polarization of the recoil proton is measured. These authors show that non-zero effects are expected in single-photon-exchange approximation. It is easy to see that the proof given in the preceding section for the vanishing of the up-down asymmetry, A , fails for the spin correlation experiments. That proof depended on the fact that the proton's spin was normal to the plane of scattering and one's ability to sum over all the other particle's spin states. In two recent papers,²² Dombey has shown that these spin-correlation measurements are $\propto G_E G_M$. Thus one can measure the relative sign of G_E and G_M . Further, one could shed more light on the speculations that the scaling law ($G_E = G_M/\mu_p = G_M/2.79$) is violated and G_E vanishes.



XBL 706-1081

Fig. 4. See reference 12.

III. EXPERIMENTAL APPARATUS AND PROCEDURE

A schematic diagram and photograph of the experimental apparatus used in our experiment appear in Figs. 5a, 5b. This experiment is conceptually very simple. One lets an electron beam hit a proton target which is polarized in a direction normal to the plane of scattering. One accurately measures the energy and intensity of the electron beam. The magnitude of the target polarization is recorded. After scattering off the target, the electron emerges into a magnetic spectrometer where its scattering angle and momentum are measured. From these kinematic quantities one calculates the "missing mass", (MM), of the unobserved hadronic state. If one neglects the electron mass

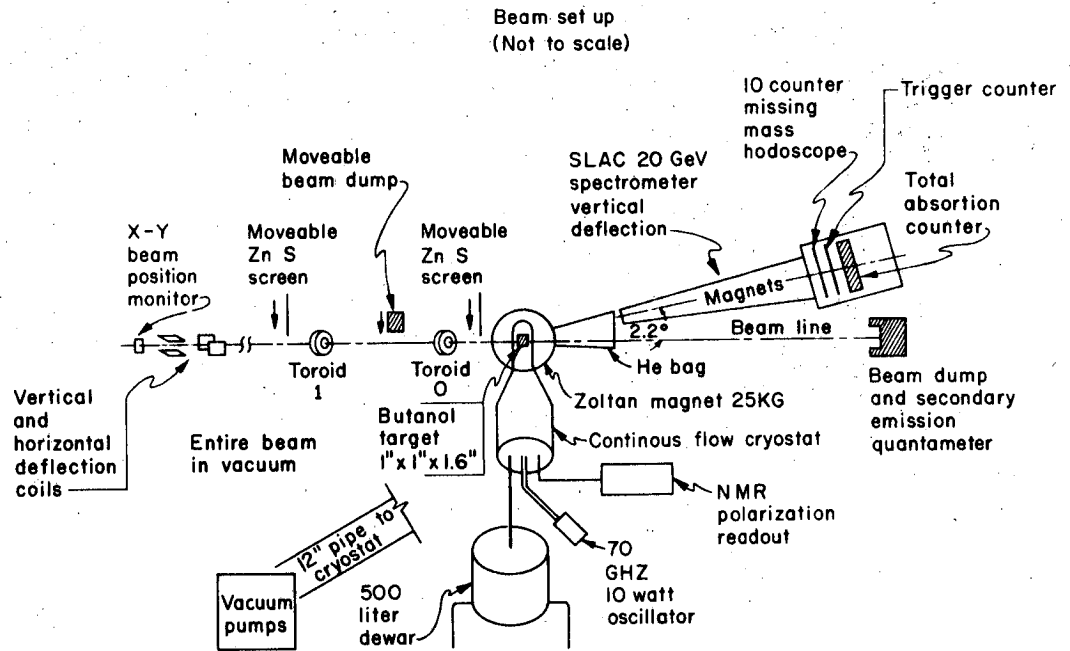
$$(MM)^2 \approx M_p^2 + 2M_p(E_0 - E') - 4E_0E'\sin^2 \frac{\theta}{2} \quad (43)$$

where E_0 = incident electron energy

E' = scattered electron energy

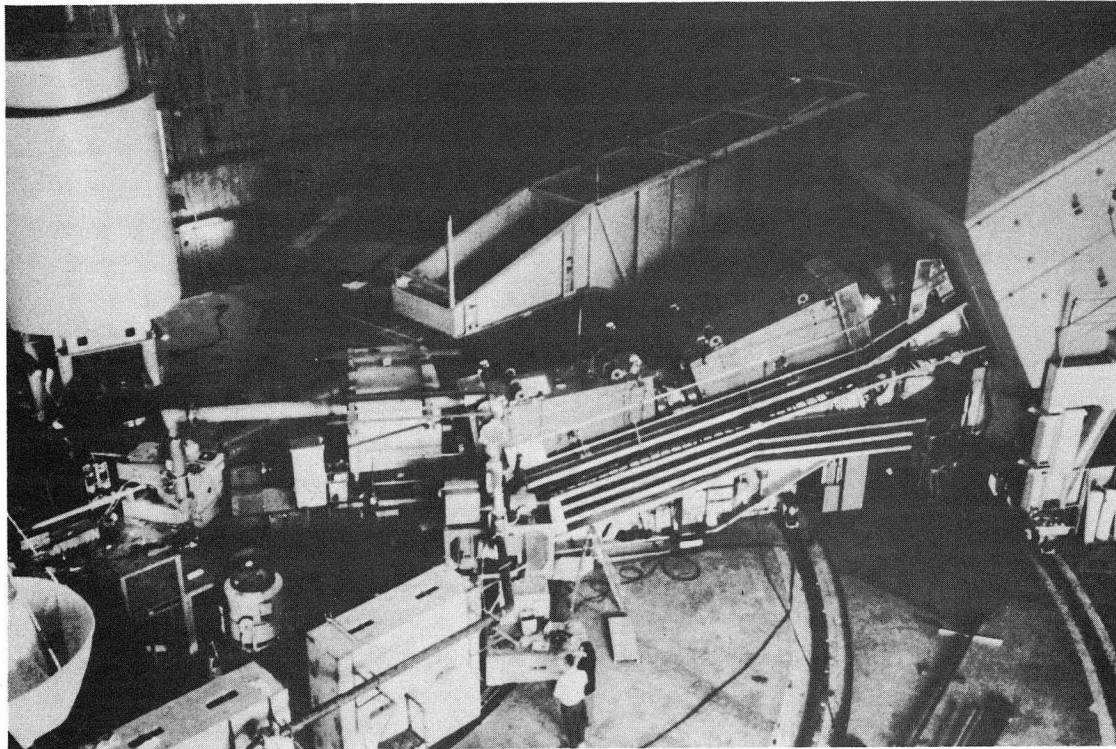
θ = electron scattering angle.

One calculates a missing-mass spectrum, i.e the experimenter calculates $\frac{d^2\sigma}{d\Omega d(MM)}$ vs. (MM) for this sign of polarization. Hence for each value of missing mass, a number $\sigma(\uparrow)$, is produced where the target is polarized in the (\uparrow) direction. Then the target polarization is reversed and another number, $\sigma(\downarrow)$, is produced for this direction of polarization, (\downarrow), for each value of missing mass. A raw asymmetry, ϵ , is calculated,



XBL6911-6279

Fig. 5a.



XBB 706-2460

Fig. 5b. The 20 GeV/c spectrometer stretches from top center toward upper right-hand corner.

$$\epsilon = \frac{\sigma(\uparrow) - \sigma(\downarrow)}{\sigma(\uparrow) + \sigma(\downarrow)}$$

The experimenter now has values of ϵ for the range of missing-mass values in which he is interested. Unfortunately, the target was not polarized 100%, and it did not consist of pure protons. Correction factors must be applied to this raw asymmetry, ϵ , to relate it to the asymmetry, A , an experimenter would see from 100%-polarized pure hydrogen. Indeed, if P_T is the target polarization, and H_F is the fraction of events one sees from the elemental hydrogen in the target

$$A = \frac{1}{|P_T|} \cdot \frac{1}{H_F} \cdot \epsilon \quad (1)$$

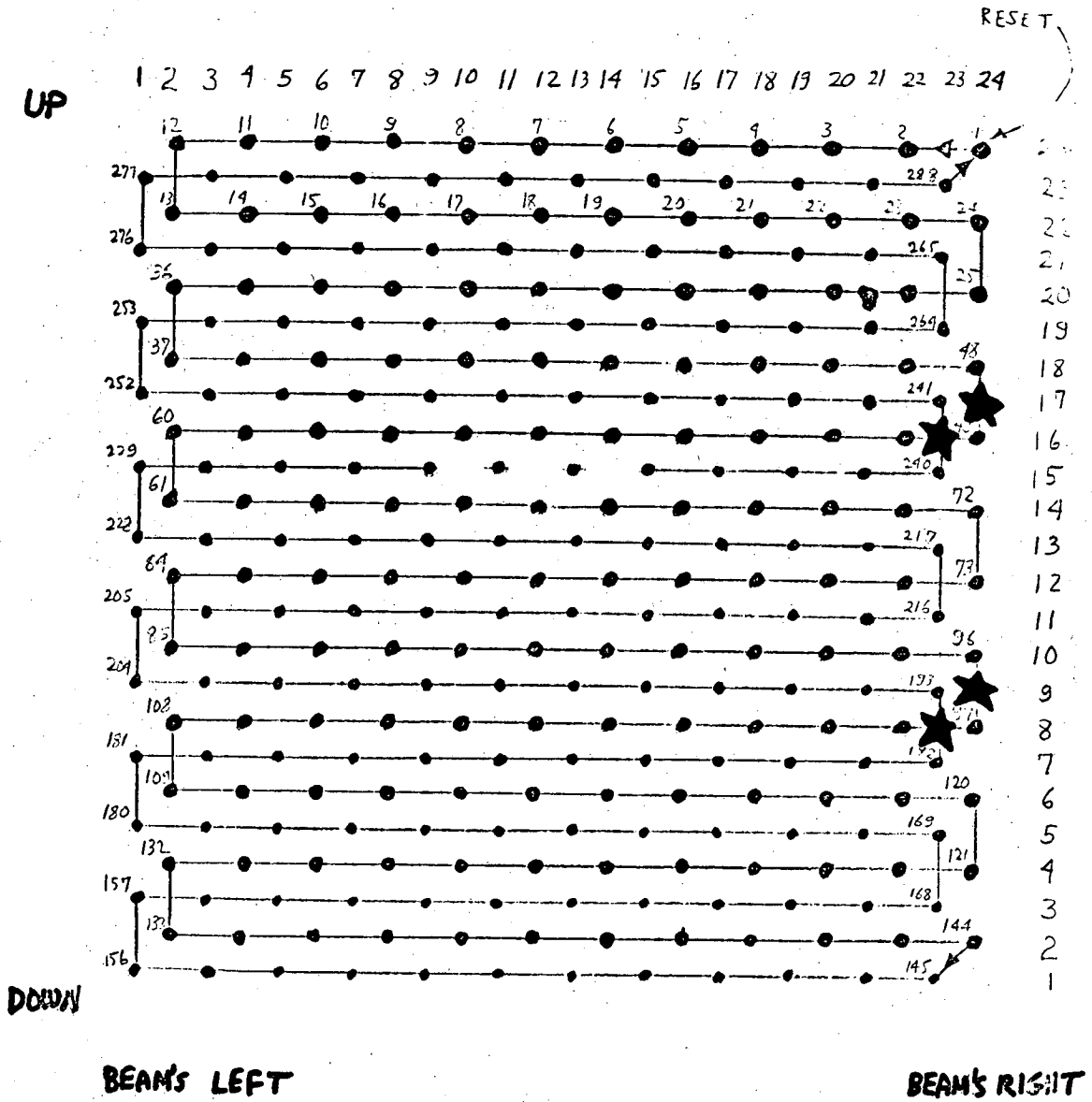
Such a "single-arm" spectrometer experiment has produced a spectrum of A vs. (MM) . This dissertation concentrates only on the elastic scattering, $(MM) \approx M_p = 938$ MeV, while a companion experiment²³ details the inelastic scattering, $(MM) > M_p$. This section will describe the methods and equipment used to accumulate the data.

A. THE ELECTRON BEAM

This experiment was performed at the SLAC 20-GeV electron accelerator²⁴ for two values of incident electron energy, 15 GeV and 18 GeV. At both of these energies the beam was collimated by slits down to $\Delta p/p = 0.2\%$. This value of $\Delta p/p$ was chosen so that the error in the measurement of (MM) due to the momentum spread in the beam would be of the same order of magnitude as the errors in (MM) due to errors in measuring the scattered electron's momentum and angle. For a value of $(MM) \approx M_p = 940$ MeV, the error in (MM) due to momentum spread in the beam was ≈ 30 -40 MeV.

Upon reaching the polarized butanol target the beam spot was approximately circular and 2-3 mm. in diameter as observed on glass slides at the target position. After each beam pulse, a pair of stepping coils, similar to Helmholtz coils, moved the beam spot to an adjacent site approximately 2.5 mm. away from the first site, on the 1" x 1" target. This "raster pattern" of horizontal and vertical sweeping of the beam appears in Fig. 6. The accelerator was run almost exclusively at 180 pulses/sec. (180 pps), with each pulse having a 1.6 μ sec. length, hence a complete cycle of the 288 sites took about 1-1/2 seconds. The spot size and sweeping pattern were designed so that the beam uniformly irradiated the butanol target. Uniform irradiation was important because the NMR apparatus, which measures the target polarization, samples essentially the volume average over the whole target. If the beam were to run selectively through only a small portion of the target, this portion would be quickly depolarized because of the beam's radiation damaging effects (see below); but the target polarization would register as non-zero, and no asymmetry from polarized protons, however large, could be measured. A contour plot of how successful the attempts at uniform irradiation were appears in Fig. 7.

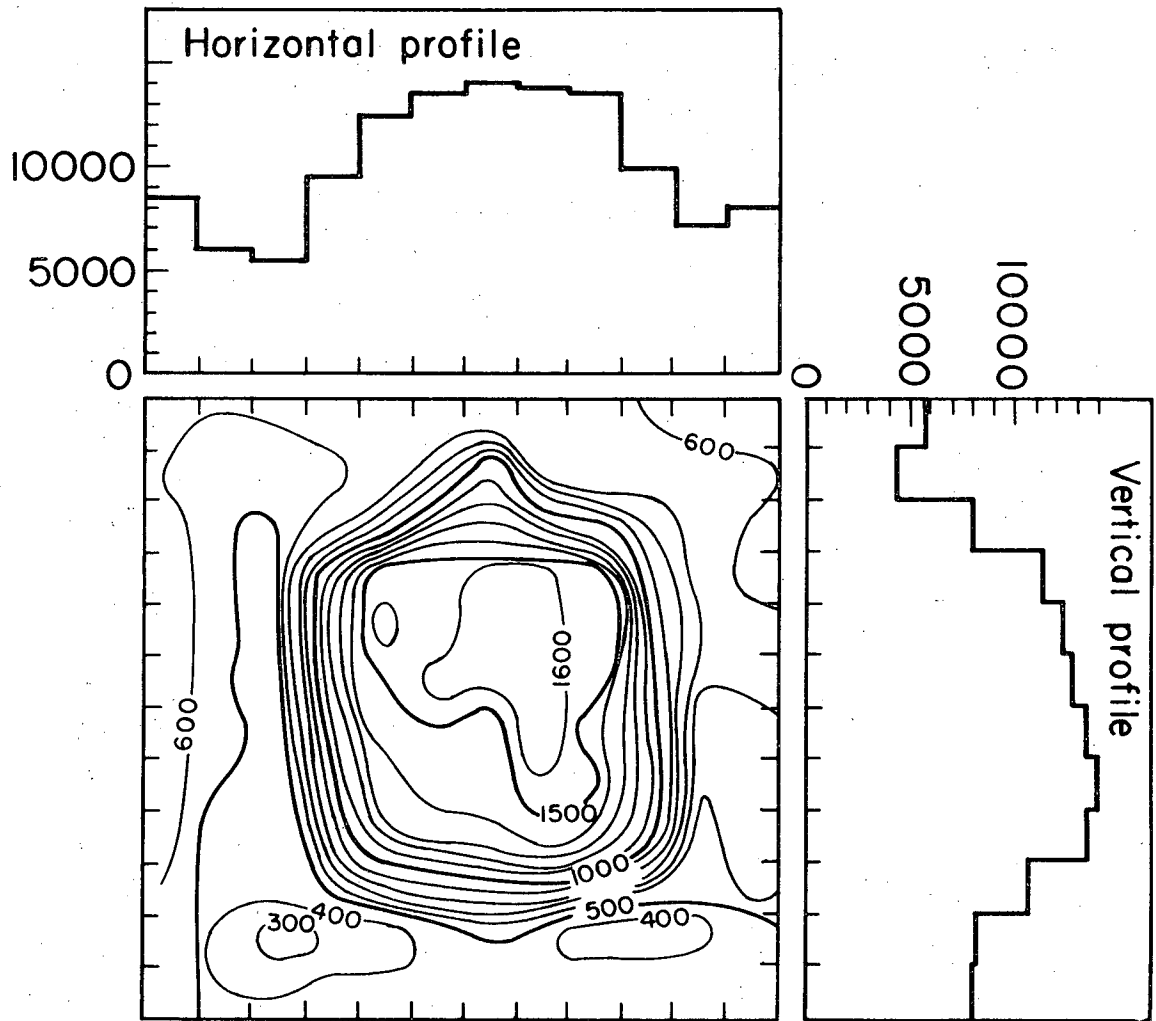
To keep the radiation damage effects within limits, we ran at an intensity of $1-2 \times 10^{11}$ electrons/sec. Even at this rate, only 0.1% of the peak SLAC intensity, we were forced to change the butanol target once per day, because the beam had destroyed the target's capacity for polarization. At these rates accidental triggers were never a problem averaging 1.2% of our total trigger rate.



"The Raster"

XBL 708-1773

Fig. 6.



XBL698-3451

Fig. 7. Beam Intensity as a function of position across the target (arbitrary units).

B. BEAM MONITORS

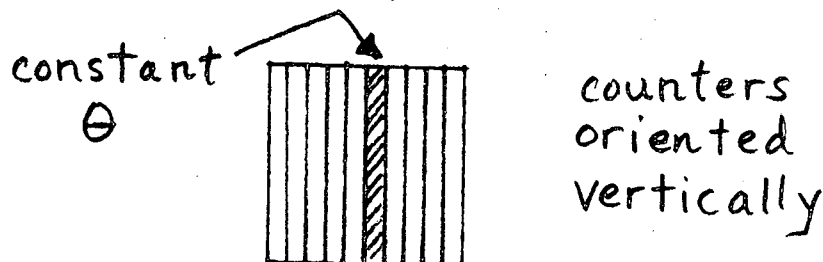
The primary beam monitors were two ferrite toroids operated in a resonant mode²⁵ in a location upstream of the target. A secondary emission quantameter,²⁶ 200 ft. downstream of the target, was used as a secondary monitor as well as a beam dump. Absolute calibration of each monitor is unnecessary, because in this experiment only the ratio of cross-sections is needed. However, errors in the asymmetry could arise if the three monitors were not consistent among themselves. For each ten second period of running (acutally six complete sweeps through the raster pattern, a period we called a "subrun"), the three monitors were required to agree with one another to 4% or better. This assured us that our errors due to monitors in any subrun were much less than our purely statistical errors in the same subrun. This can be seen quickly when one is told that a common event rate was about one event/pulse. At 180 pps this leads to 1800 events in a ten second subrun divided among ten missing-mass bins (see below) or 180 events/bin and a random error in the total counts of some 7.5% per bin, greater than 4% maximum disagreement we permitted among our monitors.

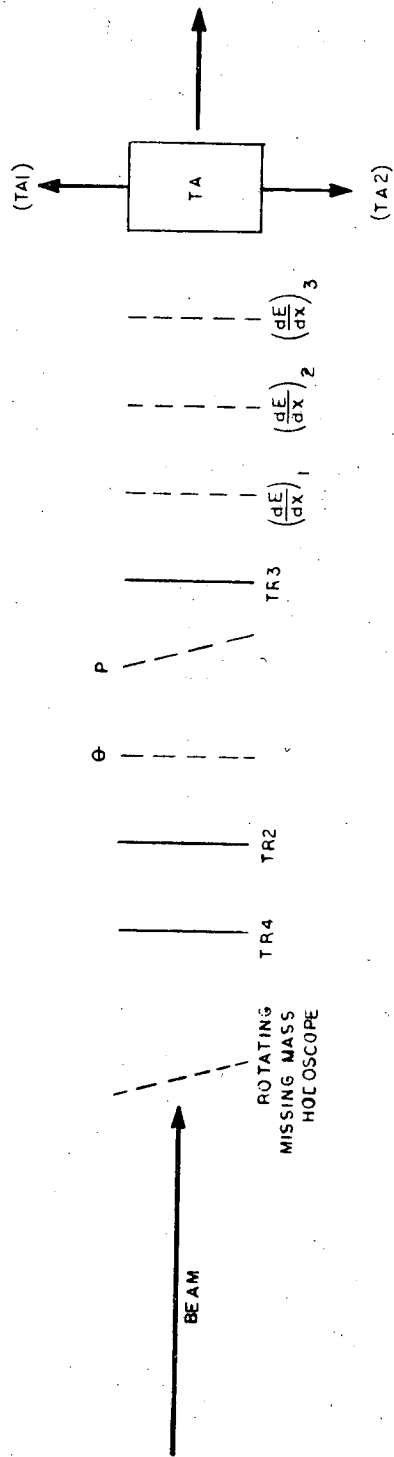
C. COUNTERS AND ELECTRONICS

Within the large 20-GeV/c spectrometer, two counter hodoscopes, the "p hodoscope" and the " θ hodoscope," to measure the momentum and angle, respectively, of a scattered electron, existed previous to the present experiment. The logic, associated electronics, computer interfacing, and programs for these hodoscopes, was such that only one trigger/pulse could be digested by the system. For this experiment, where up to 90%

in the triggers come from unpolarized carbon and oxygen nuclei in the butanol target, this system was deemed too inefficient in the low-momentum-transfer region where the counting rates are high. Thus, we constructed a third hodoscope consisting of ten scintillation counters oriented so that each counter, of dimensions 0.45" x 0.45" x 7", was oriented along a contour of constant missing mass, (MM), of the unobserved final hadronic state. A schematic diagram of the counter system appears in Fig. 8. We called the new missing mass hodoscope, along with its associated electronics, etc., "the fast system"; the old θ and p hodoscopes and its mating paraphernalia became known as "the slow system."

One can see from Eq. (43) that to have the hodoscope counters oriented along contours of constant missing mass, each counter must cover a large range of momentum values for the scattered electron (E' or p'), and a substantial range in scattering angle (θ). Thus, each counter cannot lie purely in the vertical direction, because the spectrometer brings all particles with the same scattering angle to the same vertical line.



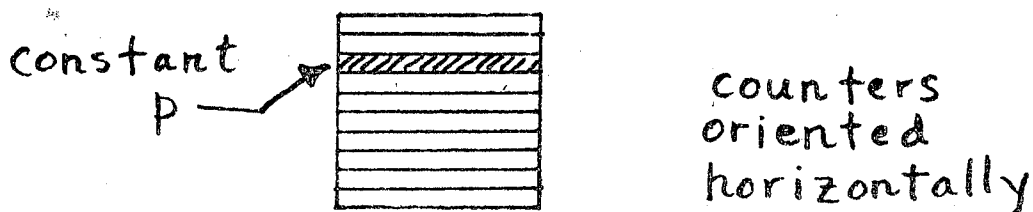


COUNTER CONFIGURATION

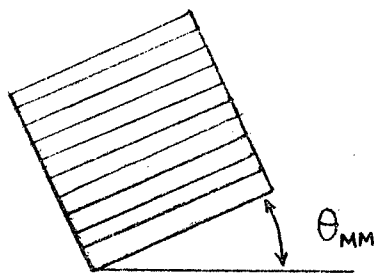
XBL 708-1778

Fig. 8.

Neither can the hodoscope counters be oriented entirely in the horizontal direction, because the spectrometer brings all particles of the same momentum to the same horizontal line.



Hence, the counters are oriented at some angle θ_{MM} .



We can quickly approximate θ_{MM} from Eq. (43) knowing the dispersion of the spectrometer in the horizontal and vertical directions. Indeed,

$$\tan \theta_{MM} = \left| \left(\frac{dy}{dx} \right)_{(MM), E_0} \right| = \frac{dy}{dp'} \cdot \left| \left(\frac{dp'}{d\theta} \right)_{(MM), E_0} \right| \cdot \frac{1}{(dx/d\theta)} \quad (44)$$

$\frac{dy}{dp'}$, = vertical dispersion in momentum in the momentum focal plane or momentum dispersion = $D_\delta = 2.826 \text{ cm}/\%$ where the $\text{cm}/\%$ means cm per 1% of the central spectrometer momentum. $\left(\frac{dx}{d\theta} \right)$ = horizontal dispersion in scattering angle in the scattering angle focal plane or angular dispersion = $D_\theta = 1.534 \text{ cm}/\text{mr}$ ²⁷

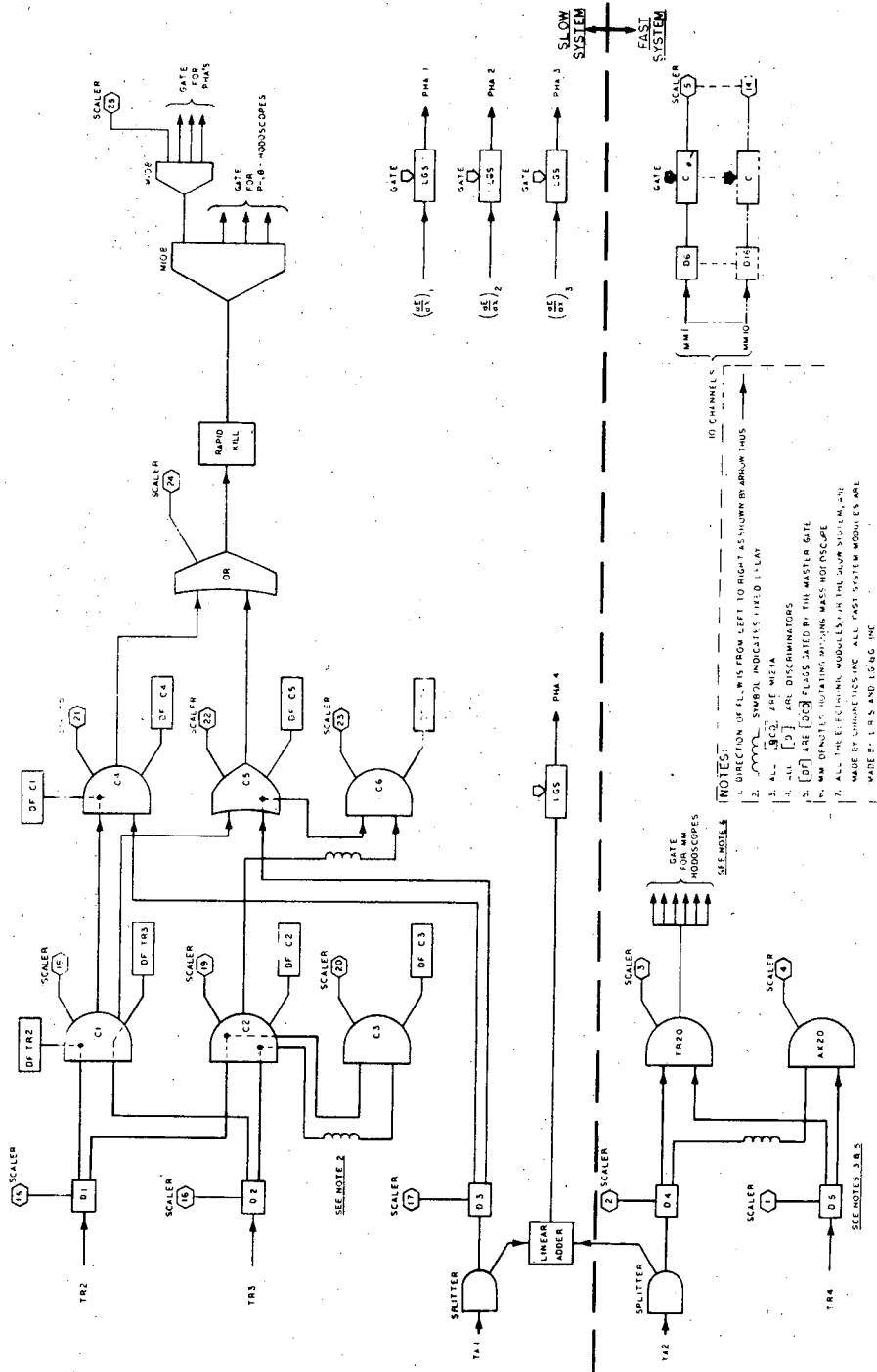
$$\left| \left(\frac{dp'}{d\theta} \right)_{(MM), E_0} \right| \approx \left(\frac{E_0}{M_p} \theta \right) E' \quad (45)$$

where we keep (MM) and E_0 constant and use the small-angle approximation in Eq. (43). At $E_0 = 18$ GeV, $\theta = 2.5^\circ$, $\theta_{MM} \approx 8^\circ$. An exact calculation gives $\theta_{MM} = 7.65^\circ$.

It must be admitted that the (MM) hodoscope could not be placed exactly at the θ and p-focal planes, because the "slow" hodoscopes remained at these planes. Indeed, we were anxious to check the "fast" system against the well-calibrated "slow" system. This fact of being out of the focal plane smears our resolution slightly, but having both systems, "fast" and "slow", enables us to make a "fast-slow" comparison and gave us great confidence in the "fast" system. Analysis of our data was performed exclusively on events taken with the "fast"(MM) hodoscope.

A diagram of the electronics and trigger logic appears in Fig. 9. For the fast system, a coincidence between a trigger counter in the spectrometer (TR4), an output from the total-absorption lead-scintillator sandwich (TA) which identified the electron, and a pulse from one of the ten missing-mass hodoscope counters generated a pulse causing one of the ten scalers which counted outputs from the ten (MM) hodoscope counters to advance.

The TA counter consisted of 16 radiation lengths of lead sandwiched between scintillator sheets. In this lead assembly, the electron emitted bremsstrahlung, the resultant γ ray formed an electron-positron pair, thus starting a shower which produces a large amount of light. The bremsstrahlung from other particles, such as muons or



XBL 708-1777

Fig. 9. Electronics and Trigger Logic.

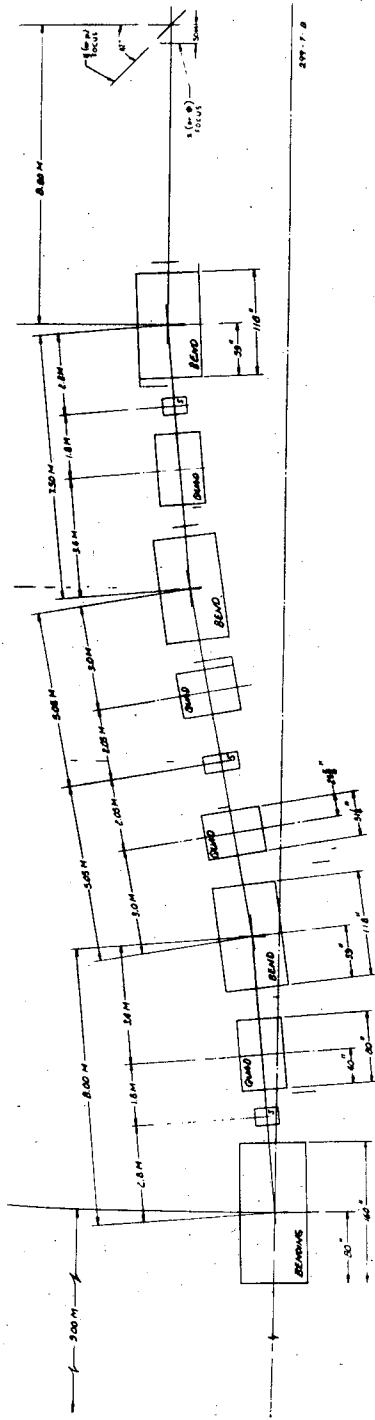
pions, will be down by factors of $(m_e/m_\mu)^2$ or $(m_e/m_\pi)^2 \approx 10^{-4} - 10^{-5}$. Hence these particles leave only minimum ionizing radiation. One then analyzes the pulse height coming from the TA output and rejects all particles whose pulse height indicates only a minimum ionizing particle passed through.

Two of the three dE/dx counters, Figs. 8 and 9, which were placed behind thicknesses of steel, were read in through the "slow"-system. Since the on-line computer recorded every fiftieth "slow" event, we were able to analyze in detail the contamination of our electron sample. We found that less than 0.2% of our events came from pions or muons. Even if the processes which produced these interlopers led to a 100% up-down asymmetry, their contribution would have an insignificant effect on our results.

D. SPECTROMETER

The final electron's momentum and scattering angle were measured in the SLAC 20-GeV/c spectrometer.²⁷ The instrument has an upward S-bend configuration with an intermediate focus. There are eleven elements in the spectrometer: 4 bending magnets (dipoles), 4 focussing magnets (quadrupoles), and 3 second-order correction magnets (sextupoles). The magnet arrangement appears in Fig. 10. Some of the design parameters are listed below:

- | | |
|---------------------|-------------------------|
| 1. Target length | $x_0 = \pm 3$ cm |
| 2. Production angle | $\theta_0 = \pm 4.5$ mr |
| 3. Target height | $y_0 = \pm 0.15$ cm |
| 4. Azimuthal angle | $\phi_0 = \pm 8$ mr |



XBL 708-1772

MAGNET ARRANGEMENT OF 20BeV/c SPECTROMETER

Fig. 10.

5. Momentum band $\pm 2\%$
6. Momentum dispersion = $D_\delta = 2.83$ cm per % momentum
7. Momentum resolution = $\pm 0.05\%$ (FWHM)
8. Solid angle = 10^{-4} steradians
9. Angular dispersion = $D_\theta = 1.53$ cm/mr
10. Angular resolution = ± 0.15 mr (FWHM)

We note that the momentum focal plane is not perpendicular to the optic axis, but inclined at an angle of 43° to the axis (see Fig. 10). The scattering angle focal plane is perpendicular to the optic axis and some 50 cm upstream from the momentum focal plane.

The matrix elements for the first-order spectrometer optics appear in Table I. The quantities x , y , θ , ϕ are defined above. z is the distance along the optic axis, or path length along the central ray. δ is $\Delta p/p$, i.e. $[p - p(\text{cent})]/[p(\text{cent})]$ where $[p(\text{cent})]$ is the momentum of the central ray. Second-order corrections, at maximum, correct the vertical and horizontal positions by less than $1/3$ cm, which corresponds to about a quarter of the width of a missing-mass bin (each MM hodoscope counter is 1.1" wide). We can safely neglect the second-order corrections and calculate orbits from first-order optics alone.

We should note one very straightforward correction to the spectrometer measurement of the scattering angle: the polarized proton target (see below) incorporates a 25 kilogauss magnet with vertical field, which bent an 18 GeV electron beam through nearly 1° . Thus it also bends the scattered electron through about $1/2^\circ$, if the electron is

Table I(a). First order transformation matrix of the S-bend spectrometer in the production angle measuring focal plane.

	$\underline{x_0}$	$\underline{\theta_0}$	$\underline{y_0}$	$\underline{\varphi_0}$	$\underline{z_0}$	$\underline{\delta_0}$
x	0.000	1.534	0.000	0.000	0.000	0.000
θ	-0.652	-0.066	0.000	0.000	0.000	0.000
y	0.000	0.000	0.757	-0.054	0.000	2.573
φ	0.000	0.000	3.410	1.078	0.000	5.061
z	0.000	0.000	0.495	0.305	1.000	0.291
δ	0.000	0.000	0.000	0.000	0.000	1.000

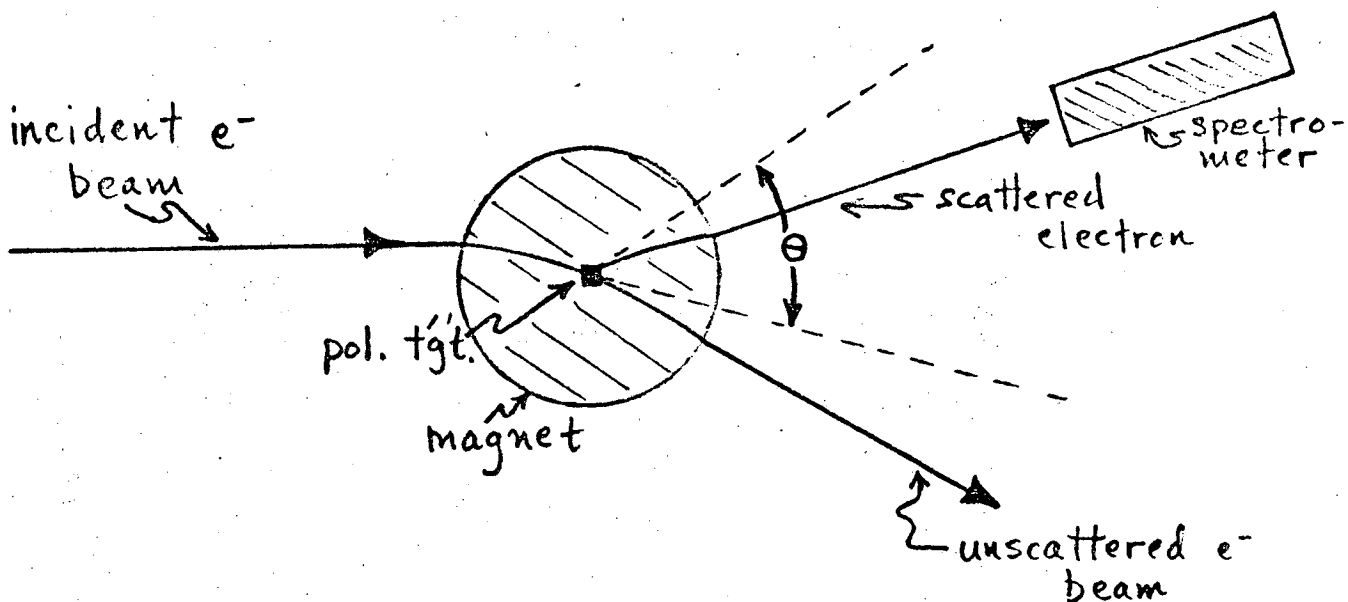
Table I(b). First order transformation matrix of the S-bend spectrometer in the momentum measuring focal plane.

	$\underline{x_0}$	$\underline{\theta_0}$	$\underline{y_0}$	$\underline{\varphi_0}$	$\underline{z_0}$	$\underline{\delta_0}$
x	0.033	1.531	0.000	0.000	0.000	0.000
θ	-0.652	-0.066	0.000	0.000	0.000	0.000
y	0.000	0.000	1.746	0.000	0.000	2.826
φ	0.000	0.000	3.410	1.078	0.000	5.061
z	0.000	0.000	0.495	0.305	1.000	0.291
δ	0.000	0.000	0.000	0.000	0.000	1.000

x, y, z in cm.

θ, φ in mr.

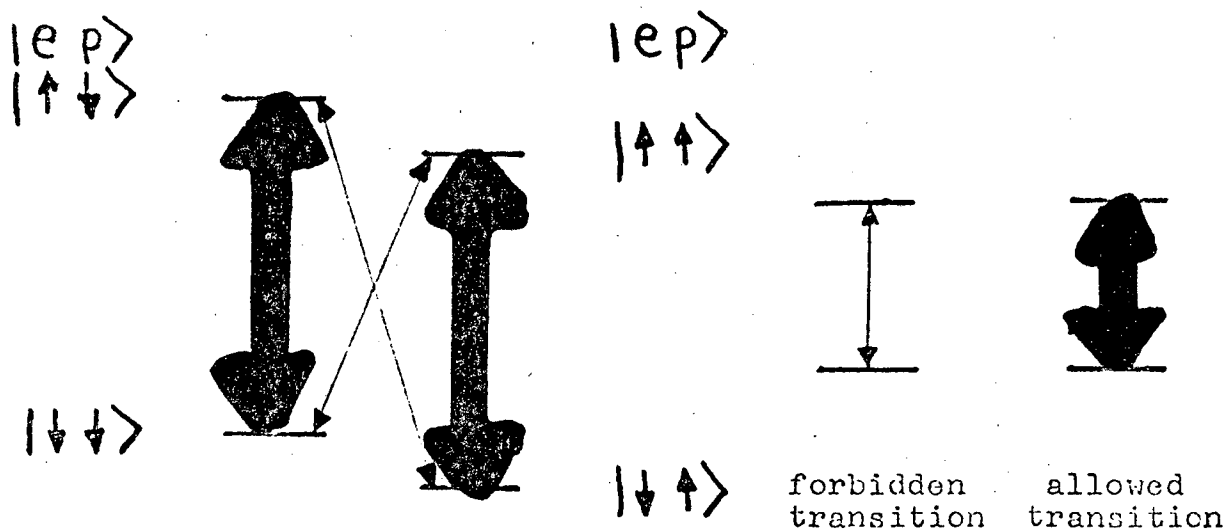
produced roughly in the forward direction. This correction is very simple to measure and easily included in the kinematics since the field of the polarized target magnet is very well mapped. A highly exaggerated view of the situation appears below.



E. POLARIZED TARGET

The principles of polarized proton targets and their applications in high energy physics have been well detailed elsewhere.²⁸ Briefly and simply, one places a substance in a high magnetic field at very low temperatures. In this particular target,²⁹ we placed a mixture of 95% 1-butanol [$\text{CH}_3(\text{CH}_2)_2\text{CH}_2\text{OH}$] and 5% distilled water doped with 2% free radical, prophyrexide [$(\text{CH}_3)_2\text{CN}(\text{:O})\text{C}(\text{:NH})\text{NHC:NH}$], in a 25.5 kilogauss magnetic field at 1.05°K . The unpaired electrons in the free

radical act like free electrons and are nearly 100% polarized, parallel to the magnetic field. The protons, nuclei of hydrogen atoms in the butanol, are only slightly polarized ($\approx 0.2\%$) because (proton magnetic moment) $\approx 1/660$ (electron magnetic moment). We remember that the other nuclei in butanol, C and O, have spin zero and are unaffected by the magnetic field. The four energy levels of this two-spin system are seen below.



The technique used to polarize the protons is to saturate the forbidden double-spin flip transitions with intense microwave energy at the specified frequency. For example, let us try to polarize the protons up, (\uparrow). We apply microwaves at the frequency to cause the transition $|\downarrow\downarrow\rangle \rightarrow |\uparrow\uparrow\rangle$. Then the state $|\uparrow\uparrow\rangle$ relaxes through an

allowed transition back down to the state $|\downarrow\uparrow\rangle$. In summary, one has tried to induce all those protons whose spins were initially down (\downarrow), into a state where their spins are up (\uparrow), and left alone all those protons whose spins were initially up, (\uparrow). The net result is that many more protons are left with spin up (\uparrow) than down, (\downarrow). Polarization by such a technique is generally called dynamic nuclear orientation,²⁸ and in particular we used the DONKEY²⁸ effect to polarize our butanol mixture. The above simple explanation is by no means the whole story, and the reader is referred to more erudite references²⁸ for a much more rigorous satisfactory discussion.

The polarized target magnet, an iron core C-magnet with circular pole faces, 8" in diameter made from Hyperco 27, a cobalt-iron alloy, produces a 25.5 kilogauss field within a 3" gap. The pole faces have been shimmed to provide a field which is uniform to 1 part in 10^4 over a one-inch cube situated at the center of the magnet gap. In this experiment, the magnet was oriented so that the field was in the vertical direction, while the plane of scattering was horizontal.

The vessel used to produce these low temperatures is a scaled up and slightly modified version of a continuous-flow horizontal cryostat designed by Pierre Roubeau.³⁰ In this device liquid helium at 1.6° K is introduced into a microwave cavity where the polarized sample sits. The helium is further cooled to 1.05° K by evaporation under the influence of a high speed pumping system ($4800 \text{ ft}^3/\text{min}$) which kept the pressure above the liquid helium around 100 micron. We estimate that the heat input from the microwave power was ≈ 0.4 watts;

further, we believe that there is a heat leak to the outside environment of about 0.7 watts. Other sources of heat gain, including the continuously used transfer line for liquid helium led to a boiloff rate of some 5 liters/hour during normal operation of the polarized target.

We observed a total liquid helium consumption of some 100 liters/16 hour - "polarized" day. 80 liters (out of 100) came from normal operation while the remaining 20 liters came during cooldown from room temperature to 1^o K.

The measurement of magnetic field was made with the NMR apparatus (see below) we used to measure the target polarization. We sent out a definite voltage signal to a radio frequency oscillator corresponding to the central frequency of that oscillator (105.5 MHz). The oscillator drove a parallel resonant circuit (see Fig. 11) which contained the butanol sample. We monitored the resonance signal from this circuit as the oscillator swept through its central frequency. We varied the magnetic field in which the sample sat until the center of the resonance signal corresponded to the central frequency of the oscillator. Then the magnetic field B was known from the relation $\omega_c = 2\mu_p B$ where ω_c = central resonance (or oscillator) frequency and μ_p = magnetic moment of the proton = 2.79 nuclear magnetrons.

We measured the temperature in the microwave cavity by measuring the resistance across a number of carbon resistors. The resistance, R, is related to the temperature, T, through the semi-empirical formula 31

$$\ln R + \frac{K}{\ln R} = A + \frac{B}{T}$$

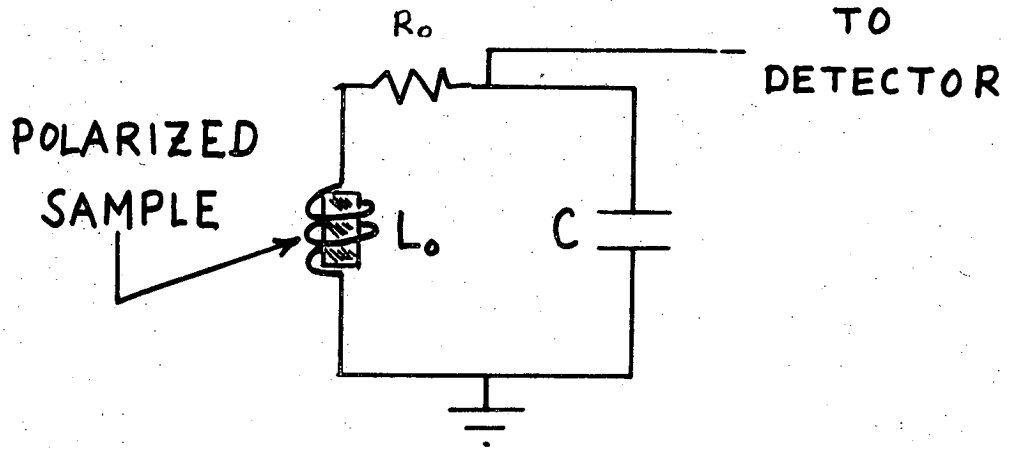


FIG. 11 a.

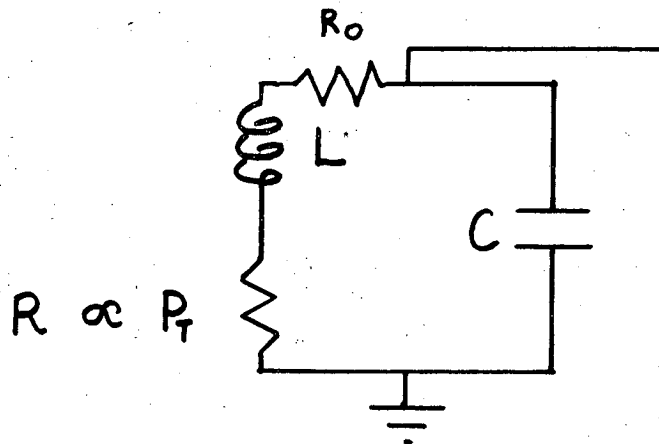


FIG. 11 b.

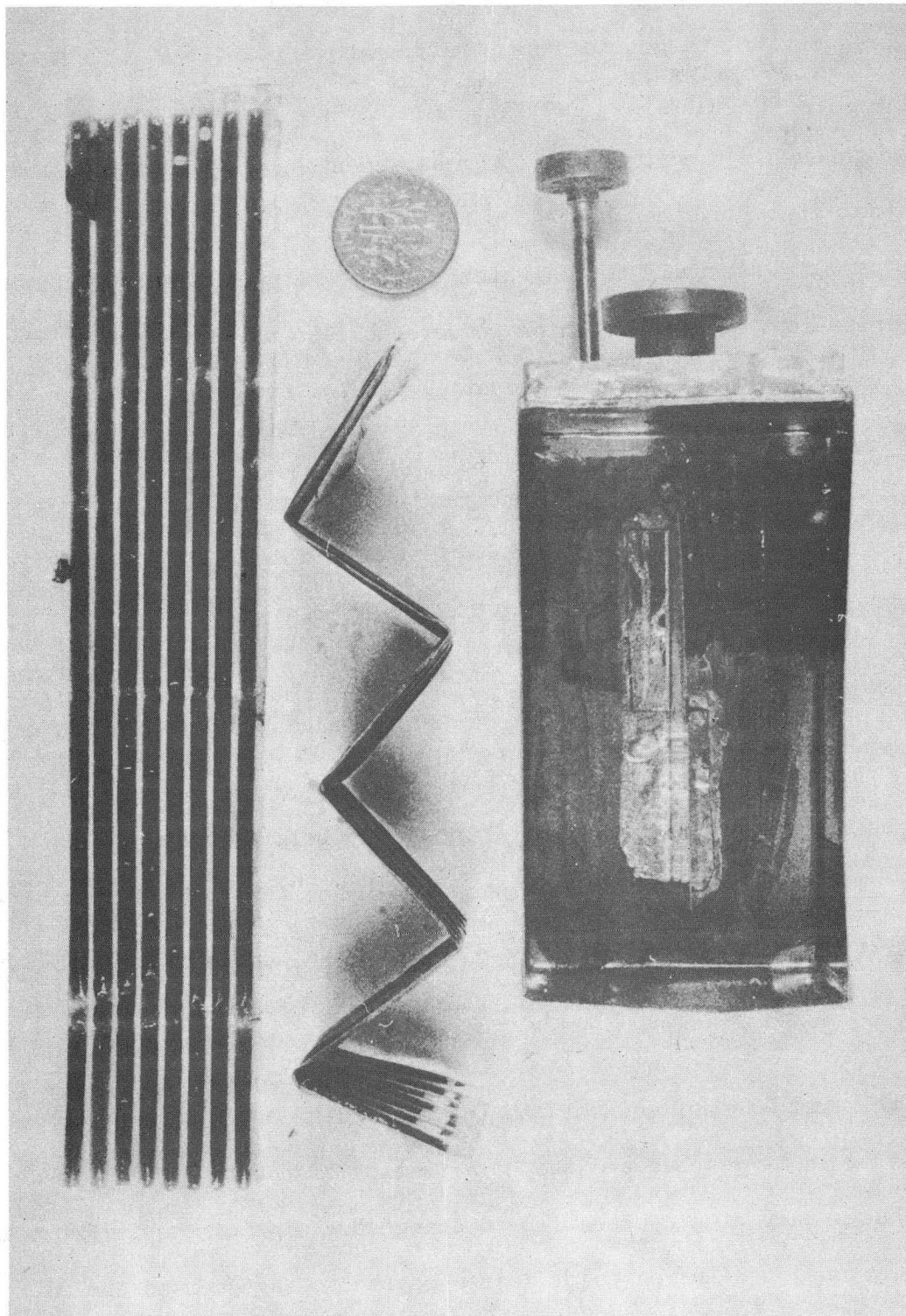
XBL 708-1771

Fig. 11. Parallel resonant circuit used in monitoring the NMR signal from the polarized target.

The constants K, A, and B were determined by measuring the resistance across each resistor at three points of known temperature: The boiling point of N_2 , the boiling point of H_2 , and the boiling point of He^4 . The use of the semi-empirical formula was checked by comparing temperatures so measured with those using the vapor pressure above liquid He^4 as seen by a McLeod gauge. The two temperatures were in excellent agreement and we believe T is known to some 2% of itself.

The thin wall copper cavity appears in Fig. 12. The top was closed off by soft soldering on a small mesh copper screen.³² The screen enabled one to pump on the liquid helium to reduce its temperature to $1.0^{\circ}K$, and still confine the microwaves to the cavity.

As previously mentioned, the target consisted of a butanol-water-porphyrin mixture. A typical target weighed 12.0 g and had a 2.5 cm x 2.5 cm cross-sectional area. This material was chosen because the fraction of hydrogen is some 13.5%, by weight, and it retains high resistance to radiation damage. Previous targets²⁸ consisted of $La_2Mg_3(NO_3)_{12} \cdot 24H_2O$ (called LMN) doped with 1% Nd. They had only 3% hydrogen by weight. But far more serious is the radiation damage problem. The polarization in LMN falls to 1/e of its initial value after some 10^{12} minimum ionizing particles/cm² pass through it.³³ Thus the beam intensity at which this experiment was performed, 10^{11} electrons/sec., would suffice to destroy an LMN target in 10 sec. The butanol target's polarization fell to 1/e of its initial value after $\approx 4 \times 10^{14}$ electrons/cm², giving lifetimes of the order of hours. Further, in butanol, one could anneal out many of the radiation induced impurities



XBB 706-1766

Fig. 12. Butanol in the ribbed plastic bags next to the micro-wave cavity.

by bringing the target to a temperature above 140°K . At this temperature a solid phase transition occurs.³⁴ We systematically ran the electron beam through a target making our measurements and gradually destroying the polarization, then heated up the target to above 140°K , and cooled the target down again to 1°K which regained most of the initial target polarization. In this fashion we were able to use one target for periods of time up to sixteen hours and still retain decent polarization. Figure 13 illustrates this procedure.

Instead of freezing the sample into one solid block, we placed the butanol mixture into six ribbed bags of $12\ \mu$ thick F.E.P.³⁵ plastic. These six bags weighed about 1.6 g. The ribbed bags presented a much larger area for the superfluid helium to cool. Hydrocarbons of the butanol type have an extremely poor heat conductivity near 1°K , and it behooves an experimenter to provide a very efficient cooling system, lest the beam heat up the sample and destroy any polarization.

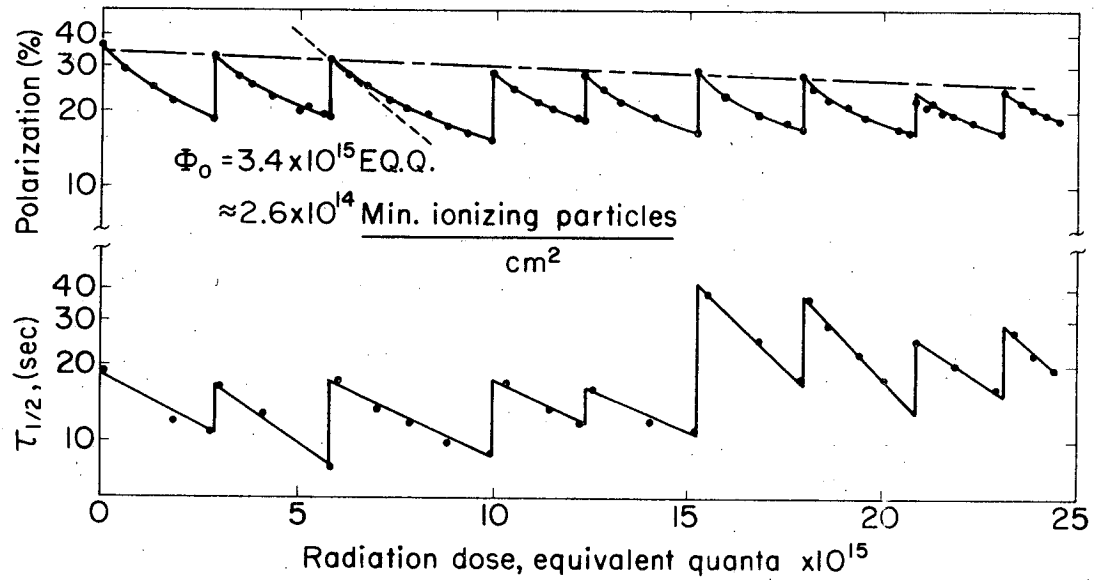
The microwave radiation used to saturate the forbidden double-spin flip transition was generated by a carcinotron tube (backward wave oscillator) operating at 71 GHz. By changing the voltage across the tube by some 200 volts, the output frequency was changed by some 0.3%. In this way the frequency of each of the two forbidden double-spin flip transitions could be reached and the polarization of the target reversed. It is thus a very simple operation to change the sign of the target polarization; one just increases or decreases the voltage across the microwave generator. It should be emphasized that no magnetic fields are reversed and no experimental apparatus is moved in changing from (\uparrow) to (\downarrow) polarization.

A typical target initially had a polarization of some 33%, and one usually took data with such a target until the polarization fell to approximately 17%, at which time we annealed it (see Fig. 13).

We measured the polarization from an NMR signal. The NMR apparatus was monitored and controlled by a small, on-line computer (PDP-5). The sign and magnitude of the polarization was sent from the PDP-5 to a much larger on-line computer (SDS 9300) which controlled all the remaining experimental apparatus, except the polarized target. The measurement technique consisted of placing the target in a coil of parallel resonant L-C circuit (see Fig. 11). We then observed the change in amplitude of an applied RF field, from a radio-frequency oscillator operating at 105.5 MHz, as this frequency is swept through the proton resonance. This measurement proceeds in two steps. First, we calibrate our NMR apparatus by observing the resonance signal from the sample at thermal equilibrium (TE), with the microwaves off. The polarization, P_{TE} , of the protons in the sample is known and is given by the Boltzmann factor

$$P_{TE} = \tanh \frac{g_p \mu_N B}{kT}$$

where $g_p \mu_N = 2.79$ nuclear magnetons, $B =$ known magnetic field, and $T =$ temperature in $^{\circ}K$. Second, we turn on the microwaves, polarize the target, and measure the resonance signal from the polarized sample. Using the known polarization associated with the calibration measurement we can relate the measured resonance curve, which was taken when the microwaves enhanced the sample, to the polarization of that butanol mixture with the microwaves on. We call the resonance signal at thermal equilibrium with microwaves off, "the TE signal," and the resonance signal with



XBL702-2355

Fig. 13. The top half of this figure shows how the target polarization falls with cumulative radiation dose and how annealing regains this polarization.

microwaves on, "the enhanced signal."

To understand how the measured resonance signal is related to the target's polarization, one must analyze the parallel L-C circuit (Fig. 11a) in greater detail. The complex impedance, Z , of a parallel L-C circuit is given by

$$\frac{1}{Z} = \frac{1}{i\omega L + R_0} + i\omega C \quad (47)$$

The presence of the oriented protons in the coil can be represented by a modification of the initial inductance, L_0 . Indeed,

$$L = L_0(1 + 4\pi\eta\chi) \quad (48)$$

where η = geometrical factor and χ = (complex) magnetic susceptibility introduced by the sample. We write $\chi = \chi' + i\chi''$ and substitute this expression along with Eq. (48) in Eq. (47) giving

$$\frac{1}{Z} = \frac{1}{i\omega L_0(1+4\pi\eta\chi') - \omega L_0 4\pi\eta\chi'' + R_0} + i\omega C \quad (49)$$

We immediately see that the term χ'' acts like a series resistor, R' , in the parallel L-C circuit (see Fig. 11b). Indeed, the complex impedance of the circuit in Fig. 11b is given by $1/Z = 1/(R_{\text{eff}} + i\omega L) + i\omega C$ with $R_{\text{eff}} = R_0 + R'$.

Many³⁶ have shown that $\chi'' \propto P_T$, hence $R' \propto P_T$, or $R_{\text{eff}} = R_0 + \alpha P_T$. One thus says that the target acts like a second series resistance $R' \propto \chi'' \propto P_T$, when he neglects the additional inductive effects of χ' .

One can manipulate these quantities to show that when driven with a constant-current source of frequency near the resonance frequency,

$$\frac{1}{V} \propto \frac{1}{|Z|} \approx \frac{R_{\text{eff}}}{\omega^2 L^2} = \frac{R_0 + R'}{\omega^2 L^2} = \frac{R_0 + \alpha(\omega)P_T}{\omega^2 L^2} \quad (50)$$

where V = voltage across the resonant circuit, and $\alpha(\omega)$ = a sharply peaked frequency-dependent factor determined by the shape of the nuclear resonance.

The measurement proceeds thusly: One, sweep the radio frequency oscillator across the resonance; Two, measure $1/V$ as a function of frequency, ω ; Three, integrate the curve of $1/V$ over all frequencies in the resonance curve (we have thus integrated out the frequency dependent factor, $\alpha(\omega)$). The above integral--the area, S , under the resonance curve of $1/V$ --is linearly dependent on P_T , i.e.

$$S = \int_{\text{resonance curve}} \frac{1}{V} d\omega \propto P_T + \text{const.} \quad (51)$$

By performing the measurement far from the resonance frequency ($\alpha(\omega) \approx 0$) one can evaluate the constant (const). One then measures three quantities: $S_{TE} = S - \text{const.}$ (S = area under the resonance curve at thermal equilibrium with microwaves off); P_{TE} (see Eq. (46)); $S_{\text{ENHANCED}} = S' - \text{const.}$ (S' = area under resonance curve with microwaves on).

$$P_{\text{ENHANCED}} = S_{\text{ENHANCED}} \left(\frac{P_{TE}}{S_{TE}} \right)$$

The PDP-5 controlled this measurement process by: One, sweeping the NMR frequency; Two, measuring and digitizing the $1/V$ signal; Three, calculating the area under the curve. The full three-step measurement of the target polarization was performed once per second. The PDP-5 also relayed the target polarization to the SDS 9300, as well as changed the voltage across the carcinotron tube to change the sign of the polarization upon command from the SDS 9300.

It must be re-emphasized that before any sample can be polarized, one must let this sample reach thermal equilibrium with microwave off ($T \approx 1^{\circ}\text{K}$, $B \approx 25 \text{ kg}$) and the experimenter must calculate P_{TE} and S_{TE} . Then one may turn the microwaves on, polarize the sample, measure S_{ENHANCED} , and use Eq. (52) to calculate $P_{\text{T}} = P_{\text{ENHANCED}}$.

F. COMPUTER CONTROL

As has been mentioned, two on-line computers were used in the data taking. A relatively large (32K memory) computer, the SDS 9300, was used to accumulate the data from scalars, monitors, pulse-height analyzers, etc. This computer controlled the data taking, as well as sampling, displaying, and checking the incoming information. A small computer, a PDP-5, controlled the polarized target and calculated the polarization. The SDS 9300 was interfaced to the PDP-5 so that the polarization could be read into the SDS 9300. The PDP-5 acted purely as a passive element, and the SDS 9300 merely updated its polarization value periodically (about once a second) and checked for any gross irregularities. A procedure which had each computer checking a number of flags was developed so that inconsistencies could not develop in the passing of information back and forth. As an example, when the SDS 9300 transferred one reading of the target's polarization into core, the SDS 9300 raised a flag. When the PDP-5 updated the measurement of the target polarization, the PDP-5 lowered that same flag. In this fashion, the SDS 9300 could tell if the polarization reading were being updated in the appointed fashion.

G. RUNNING CONDITIONS

We were forced to replace the polarized target daily due to the radiation damage problem (see above), hence each running day began with a new butanol target. The beam was then tuned for size, shape, position, and uniformity in time. During tuning the beam buried itself into a beam dump in order not to damage the target unnecessarily. Only the final position adjustment involved running the beam into the butanol target while not taking data.

When we were prepared to take data, the beam was positioned at one edge of the target using the stepping coils. After each pulse, the beam was stepped to a new position in the raster pattern (see Fig. 6). A full sweep through the raster pattern, 288 sites and thus 288 pulses, took approximately 1-1/2 seconds at the usual beam rate of 180 pps. Six full sweeps through raster pattern (≈ 10 sec) was a data-taking unit we called a subrun. Typically, after twelve subruns (≈ 2 min), the SDS 9300 sent a command to lower the beam rate to 1 pps, and a second command to the PDP-5 to change the sign of the target polarization. The PDP-5 complied by changing the voltage on the carciontron, thus changing the sign of the polarization. After approximately one minute, the target polarization had reached sufficient size (but different sign) to resume counting at 180 pps. We called the twelve subruns of data, all taken with the same sign of target polarization, a sign run. We continued in this pattern until four sign runs of data had been accumulated. We called the four sign runs a foursun. One notes, of course, that there are equal amounts of data for each sign of

polarization in a foursum. The foursum thus becomes the basic unit for data analysis, because it contains as much data for one sign of target polarization (\uparrow) as the other (\downarrow). Usually, a run consisted of four foursums, and took some 50-60 minutes to complete. One sees that the target polarization has been reversed 16 times during each run; this large number of reversals helped cancel out any asymmetries which might have arisen due to random effects. All during the run, an experimenter could select a scope display (from the SDS 9300) which sampled the data and was continually being updated. In this way, the experimenter could keep a very close check on his apparatus to see that it was performing properly. After three to four runs (3-4 hours), the electron beam had sufficiently damaged the butanol target that we were forced to anneal (see above). The heating up of the target through a resistor near the cavity and the subsequent cooldown to 1^oK took some 30-40 minutes. Most often one could anneal a target three or four times before the maximum polarization became too low for useful counting. At this point we turned the beam off and replaced the butanol target. One sees that each target lasted for some sixteen hours of every running day.

One facet of the data handling that has been omitted so far is the division of the target (for data gathering purposes) into 3 equal regions, top, middle, and bottom. The interpretation of the electron trajectory in the counter array at the end of the spectrometer is dependent upon the beam height. When the beam had been swept vertically by 1/3 inch the target image (in a certain momentum) had moved by one counter width, so the scalers were read and recorded at that

point in time. The counts were thus separately recorded for the three target regions and the final resolution in missing mass was that obtainable from a target only $1/3$ inch high.

In summary, we can see the relations among these units of data symbolically: Subrun < signrun < foursum < run < running day. The notation "subrun < signrun" means that a signrun consists of a number of subruns.

H. FRACTION OF EVENTS FROM HYDROGEN

Close to $7/8$ (by weight) of the butanol target consists of nuclei like C and O, different from the polarized protons. Roughly, then, one expects $7/8$ of his counts to come from these unpolarized heavy nuclei. One must devise a method of separating the electrons which were scattered by the polarized protons from those electrons which were scattered by the heavy elements in the target. If ϵ is the raw asymmetry in counts from the whole butanol target, we will show that the asymmetry in counts from the polarized protons is ϵ/H_F (see Eq. (1)), where H_F is the fraction of the total counts from the butanol target due to polarized protons. Indeed,

$$\epsilon = \frac{N_T(\uparrow) - N_T(\downarrow)}{N_T(\uparrow) + N_T(\downarrow)} = \frac{N_H(\uparrow) + N_B(\uparrow) - N_H(\downarrow) - N_B(\downarrow)}{N_H(\uparrow) + N_B(\uparrow) + N_H(\downarrow) + N_B(\downarrow)} \quad (53)$$

where $N_T(\uparrow)$ = total counts from butanol for the target polarized up (\uparrow); $N_H(\uparrow)$ = counts from protons for target polarized up (\uparrow); $N_B(\uparrow)$ = background counts from the unpolarized heavy elements in the target. Analogous relations exist for the target polarized down (\downarrow). Since $N_B(\uparrow) = N_B(\downarrow)$, because the heavy nuclei are unpolarized, we immediately have:

$$\epsilon = H_F \cdot \frac{N_H(\uparrow) - N_H(\downarrow)}{N_H(\uparrow) + N_H(\downarrow)} \quad (54)$$

where

$$H_F = \frac{N_H(\uparrow) + N_H(\downarrow)}{N_T(\uparrow) + N_T(\downarrow)} \quad (55)$$

We have used the fact that $N_H(\uparrow) + N_B(\uparrow) = N_T(\uparrow)$ and $N_H(\downarrow) + N_B(\downarrow) = N_T(\downarrow)$. The important point to note in the above derivation is the multiplicative nature of the relation, Eq. (54), or Eq. (1). If one is searching for a null effect, then a moderate precision in the knowledge of a multiplicative factor cannot change the significance of an answer. In this experiment we measured directly the raw asymmetry, ϵ . If ϵ were found to be significantly non-zero (which, in fact, it is not), then one could categorically say that two-photon effects had been seen. If one were asked how large was the asymmetry, A , then knowledge of the error in the multiplicative factor, the normalizing constant (normalizing to a pure hydrogen target), is vital to the calculation of the error in A . The errors in ϵ are virtually all statistical, except for a very slight correction for errors in the monitors. We saw no evidence for two-photon effects, hence we quote our errors as the statistical errors in ϵ multiplied by H_F (and P_T , of course, from Eq. (1)). The error in H_F (which was called HYFRAC) is some 20% of itself, much larger than any statistical or systematic errors in this experiment; but H_F is only a scale factor and can lead to no false claims that A is non-vanishing.

The measurement of H_F is indirect and proceeds in two steps for each individual kinematic condition.

1. One sets the spectrometer so that the elastic peak falls well

within the aperture of the missing-mass hodoscope. One takes data with three targets: butanol (unpolarized), carbon (C), and polyethylene (CH₂). The thicknesses of the C and CH₂ targets were matched to that of the butanol target by making each of the three targets have the same number of radiation lengths and the results then normalized appropriately. One performs a CH₂ - C subtraction to get a hydrogen spectrum of counts vs. (MM) at, and around, the elastic peak. One now has three spectra: N_{BU}(MM), the butanol spectrum, is the counts/monitor taken with the butanol target as a function of missing mass (MM); N_C(MM), the carbon spectrum, is the counts/monitor taken with a C target as a function of (MM); and N_H(MM), the hydrogen spectrum, is the counts/monitor gotten from the CH₂ - C subtraction as a function of (MM). Over the missing mass bins which cover only the elastic peak, one fits

$$N_{BU}(MM) = A_H N_H(MM) + A_C N_C(MM) \quad (56)$$

namely, one makes the best (in a least squares sense) choice of constants A_H and A_C so that the butanol spectrum is a linear combination of the carbon and hydrogen spectra, as taken from C and CH₂ targets at the elastic peak. The rationale behind this fit is that all heavy elements in the beam's path, whether they be Al, Cu, He, O, or, as is mostly the case, C, are simulated by the carbon spectrum; the target protons are simulated by the hydrogen spectrum.

2. For all kinematic conditions of interest, both elastic and inelastic ((MM) > 940 MeV), one takes a C spectrum, N_C, and CH₂ spectrum, and performs a CH₂ - C subtraction to get a hydrogen spectrum, N_H. One now calculates the ratio, N_C(MM)/N_H(MM) for all values of (MM); this is

the ratio of counts/monitor for carbon to hydrogen. To relate this ratio to a butanol target, we multiply by the factor A_C/A_H , gotten from fitting around the elastic peak. Indeed,

$$A_C N_C(\text{MM})/A_H N_H(\text{MM}) \quad (57)$$

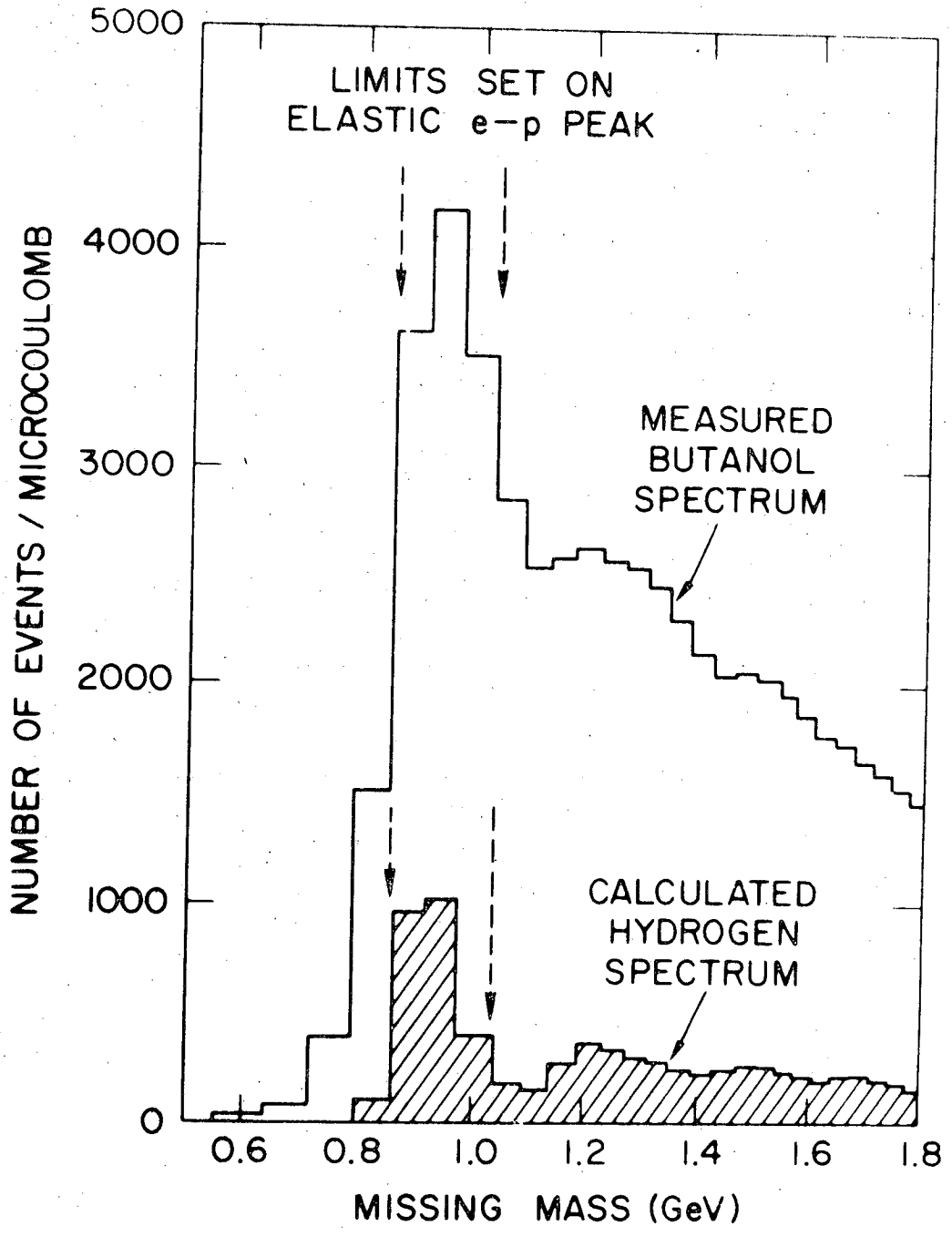
is the ratio of events from heavy elements from our butanol target set-up to that of events from protons in the butanol set-up. Finally,

$$\frac{A_H N_H(\text{MM}) + A_C N_C(\text{MM})}{A_H N_H(\text{MM})} = 1 + \frac{A_C N_C(\text{MM})}{A_H N_H(\text{MM})} = \frac{1}{H_F(\text{MM})} \quad (58)$$

Some comments are in order. The normalization of N_C and N_H is such that A_C/A_H would be unity for a pure CH_2 target. In fact, $A_C/A_H \approx 1.7$ because there were Al beam windows and walls of the cavity, liquid He cooling the butanol, some O in the butanol itself, etc.

One expects H_F to be a function of (MM) because the spectrum from hydrogen is different from the spectrum from heavy elements. For example, the spectrum from the bound protons in the carbon nuclei will be a broad bump due to those protons' Fermi momentum ³⁷ within the carbon nucleus. In fact, $H_F \approx 0.25$ near the elastic peak, $H_F \approx 0.0$ between the elastic peak and $\text{MM} \approx 1238$ MeV. Figure 14 shows a typical butanol spectrum and a hydrogen spectrum ($= H_F \times$ butanol spectrum).

The errors in H_F are some $\pm 0.2 H_F$, i.e. 20% of itself, as measured by the consistency of the measurements from day to day. Each day the elastic data from butanol were taken after the target's polarization had fallen below a useful level. From these data, plus subsidiary running with C and CH_2 , the constants A_H and A_C could be calculated for each individual target. The variation of the values for A_H and A_C give rise



XBL 708-1768

Fig. 14. The measured spectrum for scattering 15 GeV electrons (at 2.37° lab) from the polarized butanol target and a calculated spectrum for scattering from the pure hydrogen in the target ($= H_F \times$ butanol spectrum).

to the 20% error in H_F .

The fitting was done at the elastic peak because at $(MM) \approx 940$ MeV, the C and CH_2 spectra should differ by the greatest amount. This led to the most accurate $CH_2 - C$ subtraction. Nonetheless, the 20% error obtained. In a subsequent experiment³⁸ modifications of this method brought errors down to the 7% level.

IV. DATA ANALYSIS

A. Least Squares Fitting of Polarized Data

The actual calculation of $A = \frac{\epsilon}{|P_T|H_F}$ (see Eq. (1)) proceeds by making a least squares fit to Eq. (19). The detailed derivation of the fitting equations exists elsewhere³⁹ and only the salient points will be touched upon here.

Let $N_i(MM_\alpha)$ be the number of counts in the α th missing mass bin during the i th subrun. Equation (19) tells one that

$$N_i(MM_\alpha) = M_i I_o(MM_\alpha) [1 + P_i A(MM_\alpha)] + B_i(MM_\alpha) \quad (59)$$

M_i = monitor reading during the i th subrun.

P_i = target polarization during the i th subrun.

$I_o(MM_\alpha)$ = number of hydrogen counts per unit monitor for the particular target when unpolarized dependent upon differential cross section, target thickness, solid angle of counter MM_α , etc.

$A(MM_\alpha)$ = Asymmetry from pure hydrogen 100% polarized.

$B_i(MM_\alpha)$ = the background from heavy elements in the target during the i th subrun in the α th missing mass bin.

One assumes that $B_i(MM_\alpha) = b(MM_\alpha)M_i$; where $b(MM_\alpha)$ = background counts per unit monitor in the α th mass bin. From now on we will drop the MM_α dependence and restrict our attention to only one (MM) bin.

One tries to fit

$$H_i = \frac{N_i - B_i}{M_i} \quad (60)$$

= number elastic scatters/unit monitor to the form of Eq. (19), namely, $I_o(1 + P_i A)$. Hence, we use the monitor reading as weight function and make a least squares fit to Eq. (60). That is, we find the best values of I_o and A so that

$$S = \sum_i M_i [H_i - I_o(1 + P_i A)]^2$$

is a minimum. This means that $\partial S/\partial I_0 = \partial S/\partial(I_0 A) = 0$. These conditions lead to the equations:

$$\frac{\sum_i (N_i - B_i)}{\sum_i M_i} = I_0 + I_0 A \langle P_T \rangle \quad (61a)$$

$$\frac{\sum_i (N_i - B_i) P_i}{\sum_i M_i} = I_0 \langle P_T \rangle + I_0 A \langle P_T^2 \rangle \quad (61b)$$

where

$$\langle P_T^n \rangle = \left(\frac{\sum_i M_i P_i^n}{\sum_i M_i} \right).$$

Generous use has been made of Eq. (60) to reach Eqs. (61a) and (61b).

One can solve (61a) and (61b) quickly and find

$$A = \frac{e}{1 - e \langle P_T \rangle} \quad (62)$$

where

$$e = \frac{\sum_i (N_i - B_i) Q_i}{\langle Q^2 \rangle \sum_i (N_i - B_i)}$$

and

$$Q_i = P_i - \langle P_T \rangle$$

so that

$$\langle Q^2 \rangle = \langle P_T^2 \rangle - \langle P_T \rangle^2.$$

Equation (63) can be simplified by noting that $\sum_i B_i Q_i$ vanishes because the background is unpolarized (most of the heavy nuclei have spin zero). Finally we remember that our definition of HYFRAC, H_F (Eq. (55)), implies that

$H_F N_i = N_i - B_i$ so that

$$e = \frac{\sum_i N_i Q_i}{H_F \langle Q^2 \rangle (\sum_i N_i)} \quad (64)$$

and A is given by Eq. (62).

Equations (62) and (64) can be brought into the form of Eq. (1) by remembering that half of the subruns in a foursum were taken with target polarization $+ P_T$, (\uparrow), while the remaining half of the subruns had target polarization $- P_T$ (\downarrow). If the same beam intensity existed for both (\uparrow) and (\downarrow) polarization, $\langle P_T \rangle \approx 0$; then Eq. (62) becomes

$$A \approx e . \quad (65)$$

Further $Q_i \approx P_i$, so that Eq. (64) becomes

$$A \approx e \approx \frac{1}{P_T} \cdot \frac{1}{H_F} \cdot \frac{\sum_i N_i (\uparrow) - \sum_i N_i (\downarrow)}{\sum_i N_i (\uparrow) + \sum_i N_i (\downarrow)} . \quad (66)$$

This is the desired reduction to the form of Eq. (1). We emphasize that the ~~exact~~ expressions, Eqs. (62) and (64), are used to calculate the quantity A.

Errors are analyzed by using,

$$(\Delta A)^2 = \left(\frac{\partial A}{\partial e} \right)^2 (\Delta e)^2 + \left(\frac{\partial A}{\partial \langle P_T \rangle} \right)^2 (\Delta \langle P_T \rangle)^2 \quad (67)$$

$$= \frac{1}{[1 - e \langle P_T \rangle]^4} (\Delta e)^2 + \frac{e^4}{[1 - e \langle P_T \rangle]^4} (\Delta \langle P_T \rangle)^2 . \quad (68)$$

One can neglect the second term $\propto (\Delta \langle P_T \rangle)^2$, which is very small because e and $\langle P_T \rangle$ are small. Hence the error in A, ΔA , involves only the calculation of Δe . Errors in e can arise from any of four quantities: N_i (total counts in a subrun), M_i (total monitors in a subrun), P_i (the target polarization in a subrun), or H_F (see Eqs. (63), (64))). Note that Eq. (66) shows that the target polarization, P_T , and hydrogen fraction, H_F , enter only as multiplicative factors. These normalization constants can add no false non-vanishing asymmetry as emphasized above. We thus quote only errors due to the monitors, M_i , and statistical errors due to the total

number of counts, N_i . Errors in H_F and P_T will be quoted as normalization errors only.

Using the facts that $e \approx 0$, and $\langle P_T \rangle \approx 0$, the error in A due only to the statistical error in the number of counts is given by

$$\Delta A_{\text{stat}} \approx \frac{1}{H_F} \left[\frac{1}{\langle Q^2 \rangle \sum_{j=1}^v N_j} \right]^{1/2} \quad (69)$$

The error in A due only to the errors in the monitor reading is given by

$$\Delta A_{\text{Mon}} \approx \frac{1}{H_F} \left[\frac{1}{\langle Q^2 \rangle v} \right]^{1/2} \left(\frac{\Delta M}{\langle M \rangle} \right) \quad (70)$$

In Eqs. (69) and (70), $\Delta A = \Delta A(MM_\alpha)$ is the error in A in the α th missing mass bin for a given foursum. v = numbers of subruns in this foursum. $\Delta M / \langle M \rangle$ = average fractional error in the monitors for a subrun. From Eqs. (69) and (70), one sees that in any foursum

$$\frac{\Delta A_{\text{Mon}}}{\Delta A_{\text{Stat}}} \approx \left[\frac{v \sum_{j=1}^v N_j}{v} \right]^{1/2} \left(\frac{\Delta M}{\langle M \rangle} \right) \quad (71)$$

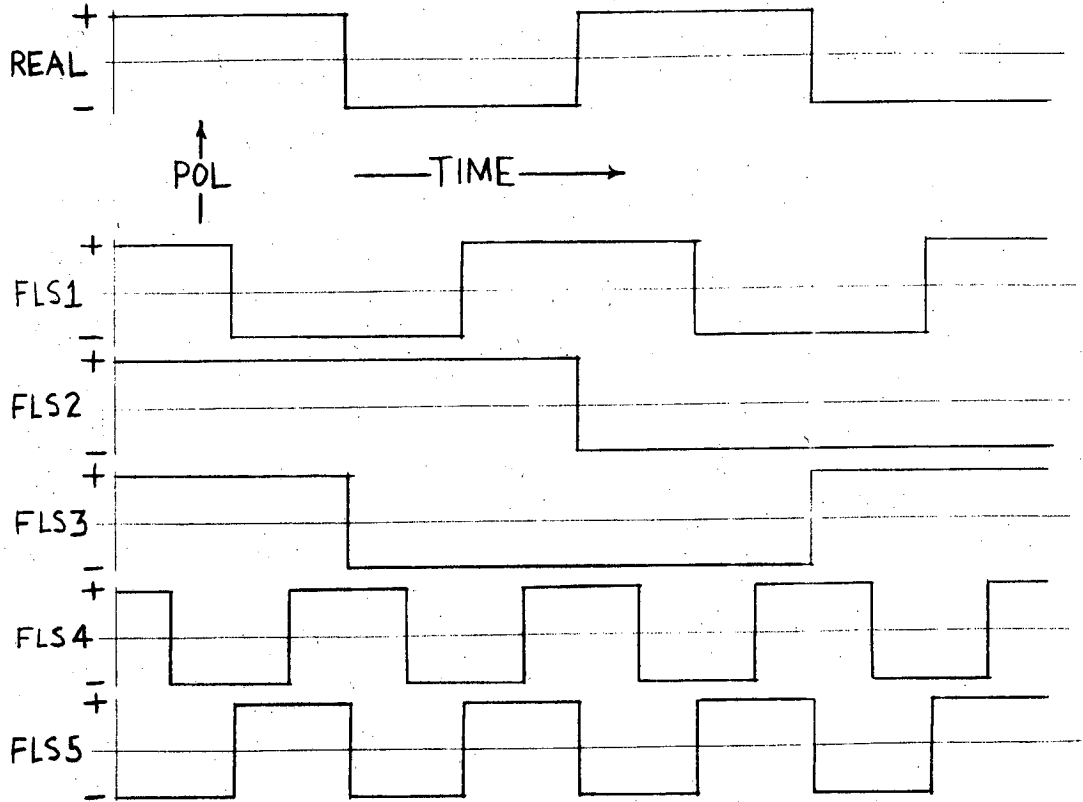
We estimate that $\Delta M / \langle M \rangle \approx 1\%$ in a subrun due to measurements of the toroids' drifts and comparisons among the three monitors. This estimate is reinforced by previous detailed studies of the toroids.²⁵ Each foursum contained 48 subruns (see above) and some 10^4 counts. Thus $\Delta A_{\text{Mon}} / \Delta A_{\text{Stat}} \approx 15\%$, and when ΔA_{Mon} and ΔA_{Stat} are added in quadrature, ΔA_{Mon} makes only a 3% correction to ΔA_{Stat} . The results quoted (in the following section) contain the errors due to the monitors, but our conclusion is that in the absence of systematic errors, virtually all of the error in this experiment is statistical.

B. Test Asymmetries

As a means of determining whether the accuracy of the data was commensurate with the statistical errors, 27 "test" asymmetries were calculated. These were based on the same data as the real asymmetry, but were calculated by pretending that the sign of the target polarization followed a pattern in time different from the real one. These patterns were chosen so that they should give a zero test asymmetry, even if the real asymmetry did not vanish. The time patterns of the real asymmetry and five of the test asymmetries are shown in Fig. 15. Note that in each of the test asymmetries shown there are equal amounts of polarization up (\uparrow) and polarization down (\downarrow). Due primarily to statistics, each of these test asymmetries has an error assigned to it by the procedure outlined above.

The test asymmetries were designed to give a measure of random errors. Complex electronic devices can, upon occasion, misbehave. A monitor could develop an altered sensitivity, or, a scaler could miscount. By constructing many test asymmetries we could obtain good evidence of the extent of random errors. Since some of the test asymmetries had time patterns with higher frequencies and some with lower frequencies than the actual polarization reversal frequency, it becomes hard to conceive of a random error that does not affect the test asymmetries. We hoped that the r.m.s. average of the test asymmetries would differ from zero only to the extent expected from the well known statistical errors.

To use the test-asymmetry data as a measure of random errors we calculated a sum over 24 missing-mass regions and over 27 test asym-



XBL 708-1770

Fig. 15. Patterns in time of the real asymmetry (REAL) and five test asymmetries (FLS1, etc.).

metries as follows:

$$C = \frac{1}{24} \cdot \frac{1}{27} \sum_{k=1}^{27} \sum_{\alpha=1}^{24} \frac{(\text{test asymmetry})_{k\alpha}^2}{(\text{error})_{k\alpha}^2}$$

For all the data at $q^2 = 0.6$, we found $C = 1.01$. We expect $C = 1.00 \pm 0.04$ if the random errors are entirely statistical. We conclude that random errors are exceedingly well given by purely statistical errors.

Even though the test asymmetries were designed as a measure of the random errors, it is possible that a systematic error may show itself there. One such systematic effect was unearthed through the analysis of the test asymmetries. The experimenters were unaware of a 60 nanosecond deadtime in the "fast" system. The source of this deadtime remains unclear to the present day. Further, by looking carefully at the monitor rate during a sign run, we discovered that the beam intensity increased by 3% from the beginning of the sign run to the end. Physically, the beam intensity increase is no doubt associated with the fact that the beam had been at 1 pps during the time the target polarization was reversing. When the sign run began the beam was immediately jumped to a rate of 180 pps. There must have been some "warm-up" problem in the accelerator itself in going from 1 pps to 180 pps.

Regardless of the causes, consideration of the pattern labeled "FLS5" in Fig. 16 coupled with the deadtime and increase in beam intensity shows that a significant effect can be produced. More monitors will be read in the second half of the sign run than the first (beam intensity increase); but fewer counts/monitor in the second half of the sign run than the first (dead time). All the counts which occur

during the second half of each sign run are labeled as coming from + (up, \uparrow) polarization when considering the "FLS5" pattern (see Fig. 16). Thus there will be systematically fewer counts/monitor for + (\uparrow) polarization, than - (\downarrow). Such an effect was indeed seen when the overall average (for 10^8 counts) of the test asymmetry, "FLS5," was shown to be about five standard deviations from zero. All the data presented in the following section were corrected for this deadtime effect, and then all the test asymmetries were very reasonable, as outline above.

C. Two Specific Systematic Checks

Checking on all systematic effects becomes a sisyphian effort. However, two checks we made are noteworthy because they are simple and obvious.

We calculated the asymmetry, A , first using one toroid as a monitor, then the other toroid as a monitor. The difference between the two values of A so garnered was less than one-fifth of the statistical error in A . Because ΔA already contains the (small) monitor error, we do not add this insignificant discrepancy to ΔA .

As noted above, data from the three target regions, top, middle, and bottom was taken separately. An asymmetry, A , was calculated for all three regions. These three asymmetries differed by amounts which were insignificant when compared with the statistical errors in each. This check is of interest because the level of liquid helium might have been lower in the microwave cavity for one sign of polarization than the other. Such a difference of liquid helium level would lead to a different asymmetry from the top target region than from the middle or bottom regions. We were concerned that such a level difference might occur if differing amounts of microwave power irradiated the sample for each sign of target polarization. To guard against this possibility, we adjusted variable attenuators in the wave guide leading to the target to equalize the power levels for $P_T(\uparrow)$ and $P_T(\downarrow)$ and we assured ourselves that the liquid helium supply rate was sufficient to overflow constantly.

The inevitable conclusion we draw from these two checks is that our errors are purely random errors, and that, as determined from the test asymmetries, the random errors are equal to the statistical errors only.

D. Normalization Errors

As the previous sections have emphasized, errors due to the target polarization (P_T in Eq. (1)) and hydrogen fraction ($H_F = \text{HYFRAC}$ in Eq. (1)) enter only as errors in normalization. These can never lead one to believe that a non-vanishing asymmetry, A , exists, if the raw asymmetry, ϵ , is consistent with zero.

We believe that the target polarization is known to less than 5% of itself. The thermal equilibrium calibrations (TE's, see above) are consistent to within 2%. Other effects within the circuitry and sampling apparatus are not well known, but can be shown to be less than 3 - 4%.⁴⁰ We thus write

$$P_T = P_{T(\text{measured})} (1.00 \pm 0.05) \quad . \quad (73)$$

We believe that H_F is known only to some 20% of itself (see above), because the determinations of H_F were consistent only within the 20% range. One might check the values of H_F by comparing ($H_F \times$ butanol spectrum) with measured values of $d\sigma/d\Omega$ for elastic e^-p scattering. Unfortunately, to make this comparison of cross sections one must consider in detail the radiative corrections to scattering from butanol, carbon, and CH_2 targets; further one must take into account the radiative effects of the Al, Cu, liquid He, and other material which the beam traverses. We have opted not to make this determination and remain content in claiming that

$$H_F = H_{F(\text{measured})} (1.00 \pm 0.20) \quad . \quad (74)$$

It is appropriate to broach the subject of radiative corrections at this point. One corrects an experimental cross section, $\sigma(\text{exp})$,

by a normalization factor, e^{δ} ; thus, $\sigma(\text{ideal}) = e^{\delta} \sigma(\text{exp})$.⁴¹ δ depends on the kinematic conditions at hand and the experimental resolution on the scattered electron's energy. We find that no radiative corrections are necessary and a detailed discussion of this point is deferred to Section VI -A.

E. Selection of Data

Each experimenter has his own idea about which data are "good" and which are "bad." Trivial checks, such as seeing that the target polarization has the correct sign and reasonable magnitude ($< 100\%$), or checking that scalars are being read correctly, catch many annoying and persistent apparatus malfunctions. Many such safeguards, too numerous to mention, were incorporated at all levels of the data taking.

When the experimental apparatus is not obviously misbehaving the line between "good" and "bad" data becomes more obscure. The general tactic for discarding data was to focus on an experimental parameter (like the accidental coincidences) and calculate the average value of this parameter for each foursum. Programs then plotted (parameter's average value)/(parameter's error) for every foursum at a given kinematic setting and calculated the mean and standard deviation (SD) from the mean for this distribution. One could choose to delete any foursum which lay beyond a certain number of SD's from the mean. For example, by setting the cut on accidental coincidences at 5 SD's, any foursum whose calculated value of (number of accidental coincidences)/(statistical error in the number of accidental coincidences) which lay greater than 5 SD's from the mean was deleted from the calculation of A.

We list the major parameters on which we made cuts in the fashion described above, and in selected cases list the numerical cutoff.

1. A cut was made on readings from the two toroids and the SEQ so that all three monitors lay within 6% of their respective mean values.
2. The beam position was monitored with an RF cavity, and a cut was made on the output from this cavity.

3. The number of triggers in the fast system was required to lie within 4 SD's of the mean.
4. Accidental coincidences - 5 SD's.
5. Each (MM) scaler was made to lie within 5 SD's of the mean over all foursums. This cut checked the scaler for reading errors (occasionally, 10^5 or 10^6 counts were added to a (MM) bin through a read error).
6. Each test asymmetry was required to be within 10 SD of zero and the combined χ^2 based on 5 test asymmetries, each collected over 12 missing-mass bins, was required to be no more than three times its statistically expected value.

With these and other less important deletions, our final cuts removed some 15% of the foursums from the data collected before calculation of A. The art of choosing just the right cut remains obscure. We reanalyzed the data under very strict criteria (50% of the foursums were deleted) and also under rather loose criteria (5% of the foursums were removed). The values of A calculated with both very strict and rather loose cuts and the value of A calculated with our final choice of cuts differ by less than one standard deviation. This evidence makes us believe that our choice of data cuts is reasonable, if still arbitrary. The data analyzed under these criteria appear in the next section.

V. Results

The results of the measurement of A appear in Table II. Two points should be made about these data: first, each value of A should be multiplied by the normalizing factors $(1.00 \pm 0.05)(1.00 \pm 0.20)$, as described in the previous section; second, we are confident that little contamination of the data occurs due to inelastic scatters because all data are well below the one-pion threshold ($MM \approx 1080$ MeV). The effects of radiative corrections on these data are discussed in the following section.

Table III shows the data summed over the bins given in Table II (see Fig. 15). To sum these asymmetries we use

$$A \pm \Delta A = \frac{\sum_i A_i / (\Delta A_i)^2}{\sum_i 1 / (\Delta A_i)^2} \pm \frac{1}{\sqrt{\sum_i 1 / (\Delta A_i)^2}}$$

and

$$\langle H_F \rangle = \frac{\sum_i N(MM_i) (H_F)_i}{\sum_i N(MM_i)}$$

where $\langle H_F \rangle$ is the value of H_F quoted in Table II.

Using Eq. (1), $A = \epsilon / |P_T| H_F$, and $\Delta A \approx \Delta \epsilon / |P_T| H_F$, where $\Delta \epsilon \approx 1 / \sqrt{\text{(Total counts)}}$ = the statistical error only, one can quickly calculate ΔA to make a rough check on the formulae of the preceding section. Indeed, consider the data for $q^2 \approx 0.6$ in Table III. Throughout the running $P_T \approx 0.22$, while $H_F = 0.16$, and $\sqrt{\text{(total counts)}} \approx 3.4 \times 10^3$. Then

$$\Delta A \approx \frac{1}{0.22} \cdot \frac{1}{0.16} \cdot \frac{1}{3.4} \times 10^{-3} \approx 0.0064$$

which is very close to 0.009, the quoted error.

We quote as our final results the data of Table III. A graph of these data as a function of q^2 (but not E_0) appears in Fig. 4. This graph compares our data (A), with other experiments (P, the polarization of the recoil nucleon).

Table II. Data for each missing mass bin.

$E_0 = 15.0 \text{ GeV}; \theta = 2.37^\circ; q^2 = 0.38 \text{ (GeV)}^2$			
<u>MM(GeV)</u>	<u>Counts</u> <u>($\times 10^6$)</u>	<u>H_F</u>	<u>$A \pm \Delta A$</u>
$0.860 \leq MM \leq 0.925$	0.501	0.26	0.024 ± 0.022
$0.925 \leq MM \leq 0.980$	0.684	0.24	-0.016 ± 0.021
$0.980 \leq MM \leq 1.040$	0.661	0.11	-0.074 ± 0.047
$E_0 = 18.0 \text{ GeV}; \theta = 2.48^\circ; q^2 = 0.59 \text{ (GeV)}^2$			
$0.830 \leq MM \leq 0.900$	1.94	0.16	-0.008 ± 0.021
$0.900 \leq MM \leq 0.975$	4.47	0.21	-0.003 ± 0.011
$0.975 \leq MM \leq 1.040$	5.22	0.11	-0.009 ± 0.020
$E_0 = 18.0 \text{ GeV}; \theta = 3.21^\circ; q^2 = 0.98 \text{ (GeV)}^2$			
$0.820 \leq MM \leq 0.900$	0.349	0.17	-0.067 ± 0.050
$0.900 \leq MM \leq 0.984$	0.585	0.29	-0.020 ± 0.022
$0.965 \leq MM \leq 1.037$	0.604	0.16	0.068 ± 0.039

Table III. Asymmetry values, A, for the elastic scattering of electrons from a polarized proton target. The errors have been calculated from counting statistics which we believe represent the total errors. A should be multiplied by normalization factors, $(1.00 \pm 0.05)(1.00 \pm 0.20)$.

Incident electron energy GeV	Electron scattering angle (deg)	Four-momentum transfer squared (GeV/c) ²	Number of elastic events ($\times 10^6$)	Hydrogen fraction H_F	Asymmetry A
15.0	2.37	0.38	1.8	0.20	-0.004 \pm 0.014
18.0	2.48	0.59	11.6	0.16	-0.005 \pm 0.009
18.0	3.21	0.98	1.5	0.21	-0.003 \pm 0.018

VII. DISCUSSION OF RESULTS

A. Radiative Corrections

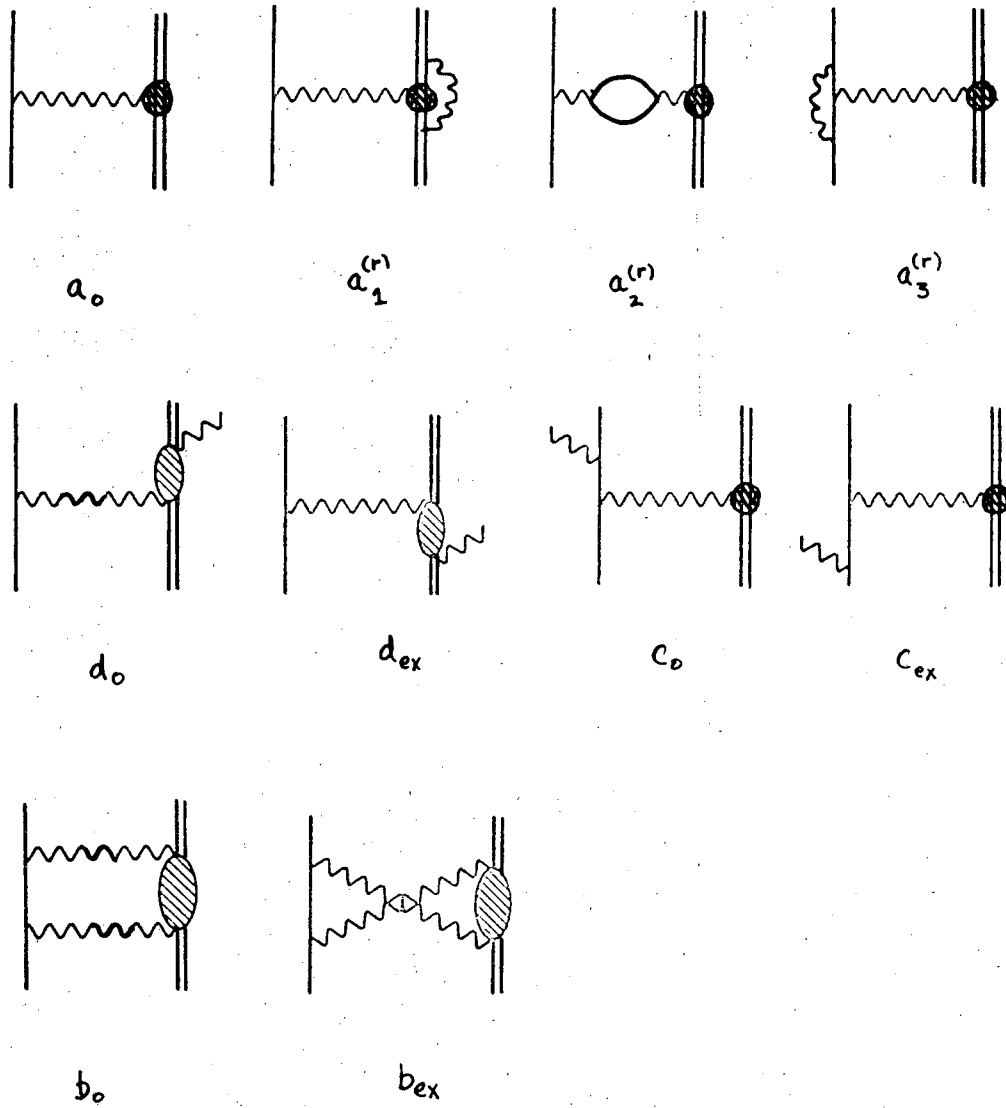
As mentioned above, no radiative corrections have been made to the data on the up-down asymmetry, A . Some justification of this must be given, since cross-section measurements are often radiatively corrected by factors of two around the elastic peak in some kinematic regions. However, in this region, $0.4(\text{GeV}/c)^2 \leq q^2 \leq 1.0(\text{GeV}/c)^2$ and $15 \text{ GeV} \leq E_0 \leq 18 \text{ GeV}$, around the elastic peak ($MM \approx 940 \text{ MeV}$) the equations of Meister and Yennie⁴¹ give corrections of about 2%. Still a 2% correction is twice the error of the most precise point which this experiment reports (at $q^2 \approx 0.6 (\text{GeV}/c)^2$ and $E_0 = 18 \text{ GeV}$).

In fact, preliminary results from the inelastic scattering from the polarized target²³ led Cahn and Tsai⁴² to consider all the second order terms in detail and see what, if any, up-down asymmetry could be attributed to the second order (two-photon) diagrams. All 1st and 2nd order diagrams appear in Fig. 16.

Diagram $a_2^{(r)}$ merely renormalizes the photon mass and $a_3^{(r)}$ simply renormalizes the e- γ -e vertex. Diagram $a_1^{(r)}$, indistinguishable from a_0 , renormalizes the p- γ -p vertex and presumably can be handled well enough by assuming that the intermediate state protons are on their respective mass shells. $a_1^{(r)}$ is thus a 2nd order correction to the proton form factors. We thus feel free to lump together a_0 , $a_1^{(r)}$, $a_2^{(r)}$, and $a_3^{(r)}$ and call them

$$a = a_0 + a_1^{(r)} + a_2^{(r)} + a_3^{(r)}$$

a is the renormalized single-photon exchange amplitude. We further call



XBL 708-1769

Fig. 16. All 1st and 2nd order diagrams in e-p scattering.

$d = d_0 + d_{ex}$, $c = c_0 + c_{ex}$, and $b = b_0 + b_{ex}$.

We calculate the cross-sections for proton spin up (\uparrow) and spin down (\downarrow).

$$\sigma(\uparrow) = |a(\uparrow) + b(\uparrow)|^2 + |c(\uparrow) + d(\uparrow)|^2$$

and a similar expression for $\sigma(\downarrow)$. Finally one remembers that

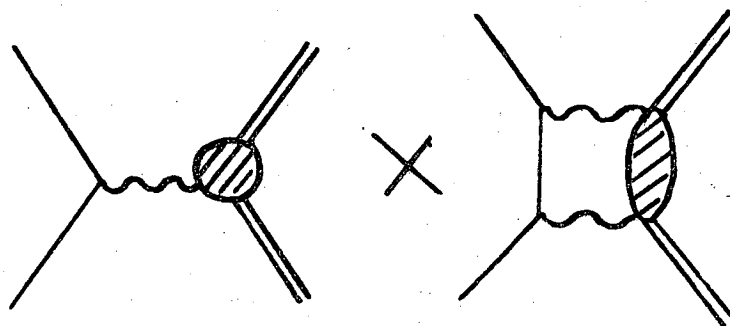
$$|a(\uparrow)|^2 = |a(\downarrow)|^2, \text{ so that}$$

$$\begin{aligned} A &= \frac{\sigma(\uparrow) - \sigma(\downarrow)}{\sigma(\uparrow) + \sigma(\downarrow)} \\ &\approx \frac{1}{2|a|^2} \left[2\text{Re}[b^*(\uparrow) - b^*(\downarrow)]a + [|c(\uparrow)|^2 - |c(\downarrow)|^2] + [|d(\uparrow)|^2 - |d(\downarrow)|^2] \right. \\ &\quad \left. + 2 \text{Re}[c(\uparrow)d^*(\uparrow) - c(\downarrow)d^*(\downarrow)] \right] \end{aligned}$$

Cahn and Tsai⁴ were able to show that the terms involving $|c(\uparrow)|^2$, $|c(\downarrow)|^2$, $|d(\uparrow)|^2$, and $|d(\downarrow)|^2$ could not contribute to any up-down asymmetry. This left only two interference terms: the proton bremsstrahlung-electron-bremsstrahlung term and the single photon-double photon contribution. The above two authors attempted to evaluate both of these terms in the region $1080 \text{ MeV} \leq (MM) \leq 1238 \text{ MeV}$. In the case of the proton bremsstrahlung-electron bremsstrahlung term, $2\text{Re}[c(\uparrow)d^*(\uparrow) - c(\downarrow)d^*(\downarrow)]$, their calculation showed this contribution to be utterly negligible. Cahn and Tsai's calculation can be applied without alteration to the elastic case ($(MM) \approx M_p$), so one feels confident in neglecting this bremsstrahlung-bremsstrahlung interference term. Only the single photon-double photon interference term remains, and no bremsstrahlung or radiative corrections to the up-down asymmetry, A.

Cahn and Tsai pointed out one interesting fact about the two-photon

exchange diagram. Only diagram b_0 (see Fig. 17) has an imaginary part, while diagram b_{ex} has only a real part. This unexpected vanishing of the $\text{Im}(b_{ex})$ occurs because of the unitarity relation, $i(T - T^\dagger) = TT^\dagger$. Indeed, $i(T - T^\dagger)_{fi}$ is related to $\text{Im}(T_{fi})$; while $(TT^\dagger)_{fi} = \sum_n T_{fn} T_{in}^*$, where the sum is over all real, on the mass shell, intermediate states, $|n\rangle$. b_{ex} (in Fig. 17) is a diagram in which no intermediate state is kinematically possible, hence $\text{Im}(b_{ex}) = 0$. Thus only the interference term between b_0 and a need be calculated.



B. Other Experiments

From the results of this experiment and from the measurements of Mar et al.,⁴ on the real part of two-photon exchange amplitudes, one can conclude that the higher-order contributions to elastic electron-proton scattering have been found to lie between 0 and order α , in agreement with the theoretical estimates.

A further experiment has been performed near this kinematic region to look for two-photon-exchange contributions to elastic muon-proton scattering.⁴³ This experiment looked for a difference between $\sigma(\mu^+ p)$

and $\sigma(\mu^-p)$, i.e. measured the real part of two photon exchange contributions to μ -p scattering. The experimenters found that $\sigma(\mu^+p) = \sigma(\mu^-p)$, consistent with their experimental errors of 2%. No experiment has been performed which might look for the imaginary part of two photon exchange with a polarization or up-down asymmetry measurement in $\mu^\pm p$ scattering. No such experiment has even been remotely considered, because the counting rates would be much too low for a significant test with the present intensity of muon beams.

ACKNOWLEDGMENTS

It is easy to thank the three faculty members who guided my research.

Professor Owen Chamberlain's insight into physical situations still fills me with awe. The hours I have spent with him have been fruitful and fulfilling. He has accepted me and his other students as equals, true colleagues, and never anything less. My only regret in four years with Professor Chamberlain is that I could not spend more time with him.

Professor Herbert Steiner has been a friend as well as a mentor. Though he was unable to participate in the work this dissertation reports, his interest and encouragement has always been at a high level, indeed sometimes overwhelming.

Professor Gilbert Shapiro participated in most phases of the work this dissertation reports, giving his advice lavishly and selflessly.

Two co-workers, Dr. Howard Weisberg and Michel Borghini participated very actively in this work. Dr. Weisberg constantly goaded those around him to greater effort. His hard work and attention to detail heightened this work's quality. Michel Borghini is the world's greatest polarizer of protons. To work with the master was an unexpected bonus of this experiment. Michel's quiet humor kept his colleagues waiting for every tidbit.

My closest companions in physics of the last four years have been my fellow graduate students, William Gorn, Charles Morehouse, Peter Robrish, Stephen Rock, and Stephen Shannon. Messrs. Morehouse, Robrish, and Shannon helped me in an early, abortive, and dreadfully frustrating attempt to perform this experiment with another apparatus. Their loyalty commands my deep respect. Special thanks must go to my closest

collaborator, Stephen Rock, who carried the lion's share of the data analysis and experimental burden in our joint venture. Without his help this thesis could not have been written.

Raymond Zoltan Fuzesy, our group's outstanding technician, was a friend and willing partner in crime. His common sense tided me over some rough spots of the last four years. John Jaros, another graduate student, ably assisted Mr. Fuzesy at SLAC.

Mrs. Rosemary Fowell, our group's secretary, has been my confidante since 1966. Her able assistance in this manuscript is evident throughout; but her warm personality has been more important to my sanity. I must also thank Mr. Joe Noble and Miss Miriam Machlis for aid in typing this thesis.

I express my gratitude for the hard work and cooperation of my SLAC colleagues, R.L.A. Cottrell, J. Litt, L.W. Mo, and R.E. Taylor, plus the legion of support personnel from their laboratory who aided us.

I sadly acknowledge that my wife, Betsy, and my daughters, Daphne and Rachel, have suffered through my formal student years. I hope their relief at the cessation of this apprenticeship is appropriate, and that I can repay the debt I owe them. I hope subsequent students can treat more humanely those closest to them and still remain within the often inhuman confines of their discipline.

APPENDIX I

The purpose of this appendix is to formalize the argument that current conservation insures a time-reversal-invariant amplitude for elastic scattering if the interaction occurs purely through a single photon exchange.⁴⁴ The development is rather formal and a brief outline of the steps in the proof may help the reader through the maze of Dirac algebra. First, one uses invariance principles to construct the most general form of the proton current operator. This involves three form factors. Second, one uses hermiticity to prove that all the form factors so defined are real. Third, one uses time reversal invariance and rotational properties of some Dirac matrix elements to show that one of these same form factors must be pure imaginary. Fourth, one draws the conclusion from the above demonstrations that if a physicist wants a time-reversal invariant, hermitian current then the form factor which is to be simultaneously pure real and pure imaginary must vanish. Clearly, if the form factor in question did not vanish, it would have to be real (hermiticity), and thus violate time-reversal invariance. The final step in the proof is the realization that current conservation would make this time-reversal violating form factor vanish anyway for elastic scattering.

To construct the most general vector to represent the proton current, one uses the available vectors and Dirac matrices. This construction is quite familiar,^{2,9} so we reproduce only the necessary results.

The matrix element, $\langle p_f^{(p)} | J_\mu^{(p)} | p_i^{(p)} \rangle$, can depend only on scalars formed from $p_f^{(p)}$, $p_i^{(p)}$, and Dirac matrices. The only independent scalar is $q^2 = (p_f^{(p)} - p_i^{(p)})^2 = (4\text{-momentum transfer})^2$.

The only vector which satisfies the constraints of Lorentz invariance and parity conservation (which the electromagnetic current must obey) is

$$\bar{u}(p_f^{(p)}) [A_1(q^2)\gamma_\mu + A_2(q^2)P_\mu + i A_3(q^2)q_\mu] u(p_i^{(p)}) \quad (A.1)$$

We have used the fact that free particle proton states satisfy the free particle Dirac equation. A_1 , A_2 , and A_3 are the three form factors. $P_\mu = (p_f^{(p)} + p_i^{(p)})_\mu$ and $q_\mu = (p_f^{(p)} - p_i^{(p)})_\mu$. The use of the free particle Dirac equation permits one to use two identities which are useful in the derivation of Eq. (A.1):

$$\bar{u}(p_f^{(p)}) [i \sigma_{\mu\nu} P_\nu] u(p_i^{(p)}) = \bar{u}(p_f^{(p)}) [-q_\mu] u(p_i^{(p)}) \quad (A.2)$$

$$\bar{u}(p_f^{(p)}) [i \sigma_{\mu\nu} q_\nu] u(p_i^{(p)}) = \bar{u}(p_f^{(p)}) [2M_p \gamma_\mu - P_\mu] u(p_i^{(p)}) \quad (A.3)$$

Equation (A.3) is known as the "Gordon decomposition of the current"⁹ and $\sigma_{\mu\nu} = \frac{i}{2}(\gamma_\mu \gamma_\nu - \gamma_\nu \gamma_\mu)$.

We return to Eq. (A.1) and use the fact that the proton current operator, $J_\mu^{(p)}$, is Hermitian. Then, taking $J_0^{(p)}$ as an example,

$$\begin{aligned} & \bar{u}(p_i^{(p)}) [A_1^* \gamma_0 + A_2^* P_0 - i A_3^* q_0] u(p_f^{(p)}) \\ &= \bar{u}(p_f^{(p)}) [A_1 \gamma_0 + A_2 P_0 + i A_3 q_0] u(p_i^{(p)})^* \\ &= \sqrt{\frac{E_f^{(p)}}{M_p} \frac{E_i^{(p)}}{M_p}} \langle p_f | J_0^{(p)} | p_i \rangle^* \\ &= \sqrt{\frac{E_f^{(p)}}{M_p} \frac{E_i^{(p)}}{M_p}} \langle p_i | J_0^{(p)} | p_f \rangle \\ &= \bar{u}(p_i^{(p)}) [A_1 \gamma_0 + A_2 P_0' + i A_3 q_0'] u(p_i^{(p)}) \quad (A.4) \end{aligned}$$

We have called $P'_\mu = (p_i^{(p)} + p_f^{(p)})_\mu = P_\mu$; while $q'_\mu = (p_i^{(p)} - p_f^{(p)})_\mu = -q_\mu$. Hence, $q'^2 = q^2$, so that $A_1^* = A_1$, $A_2^* = A_2$, and $A_3^* = A_3$ or A_1, A_2 , and A_3 are pure real, because $J_\mu^{(p)}$ is Hermitian. The above proof hinges on the fact that $\gamma_0 = \gamma_0^\dagger$ (because $\gamma_\mu = (\beta, \beta\vec{\alpha})$) and the careful attention paid to the definition of q_μ in Eq. (A.1).

Let us now apply the time reversal operator, \mathcal{J} , to Eq. (A.1). We take, for example, the space components of $J_\mu^{(p)}$, $\mu = 1, 2, 3$

$$\mathcal{J} J_k^{(p)} \mathcal{J}^{-1} = - J_k^{(p)} \quad k = 1, 2, 3 \quad (\text{A.5})$$

if the electromagnetic interaction of hadrons is time reversal invariant.

Instead of applying simply \mathcal{J} , we find the manipulations simpler if we apply the combination $R_\pi \mathcal{J}$, where R_π is the rotation operator through angle π about an axis perpendicular to the plane of scattering (\hat{n} = normal to plane of scattering is parallel to $\vec{p}_i^{(p)} \times \vec{p}_f^{(p)}$). We note that

$$(R_\pi \mathcal{J}) J_k^{(p)} (R_\pi \mathcal{J})^{-1} = + J_k^{(p)} \quad (\text{A.6})$$

if the k^{th} direction is not along \hat{n} ; also

$$R_\pi \mathcal{J} u_\lambda(p) = u_\lambda(p) \quad (\text{A.7})$$

if $u_\lambda(p)$ is a state of fixed helicity λ , ($\lambda = \vec{\sigma} \cdot \vec{p}$), because a) $\vec{\sigma} \cdot \vec{p}$ is rotationally invariant as well as time reversal invariant b) \mathcal{J} reverses \vec{p} , but R_π returns \vec{p} to its original direction. Then

$$\begin{aligned} & \langle p_f | J_k^{(p)} | p_i \rangle \\ &= \bar{u}_{\lambda_f}(p_f) [A_1 \gamma_k + A_2 P_k + i A_3 q_k] u_{\lambda_i}(p_i) \\ &= \bar{u}_{\lambda_f}(p_f) [(R_\pi \mathcal{J})^{-1} (R_\pi \mathcal{J})] [A_1 \gamma_k + A_2 P_k + i A_3 q_k] \cdot [(R_\pi \mathcal{J})^{-1} (R_\pi \mathcal{J})] u_{\lambda_i}(p_i) \end{aligned}$$

$$\begin{aligned}
 & \langle p_f | J_k^{(p)} | p_i \rangle \\
 &= \bar{u}_{\lambda_f}(p_f) \left\{ (R_\pi \mathcal{J}) [A_1 \gamma_k + A_2 P_k + i A_3 q_k] (R_\pi \mathcal{J})^{-1} \right\} u_{\lambda_i}(p_i) \\
 &= \bar{u}_{\lambda_f}(p_f) R_\pi \left\{ \mathcal{J} [A_1 \gamma_k + A_2 P_k + A_3 q_k] \mathcal{J}^{-1} \right\} R_\pi^{-1} u_{\lambda_i}(p_i) \\
 &= \bar{u}_{\lambda_f}(p_f) R_\pi [-A_1^* \gamma_k + A_2^* P_k - i A_3^* q_k] R_\pi^{-1} u_{\lambda_i}(p_i)
 \end{aligned}$$

where the last line follows because \mathcal{J} is antiunitary and the fact that $\mathcal{J} \gamma_k \mathcal{J}^{-1} = -\gamma_k$.⁹ Finally, we use the fact that $\bar{u}_{\lambda_f}(p_f) \gamma_k u_{\lambda_i}(p_i)$ transforms like a vector under rotations. Thus,

$$\bar{u}_{\lambda_f}(p_f) R_\pi \gamma_k R_\pi^{-1} u_{\lambda_i}(p_i) = -\bar{u}_{\lambda_f}(p_f) \gamma_k u_{\lambda_i}(p_i)$$

because

$$\bar{u}_{\lambda_f}(p_f) \gamma_k u_{\lambda_i}(p_i)$$

vanishes if the k th direction is along \hat{n} . Thus

$$\begin{aligned}
 & \bar{u}_{\lambda_f}(p_f) [A_1^* \gamma_k + A_2^* P_k - i A_3^* q_k] u_{\lambda_i}(p_i) \\
 &= \bar{u}_{\lambda_f}(p_f) [A_1 \gamma_k + A_2 P_k + i A_3 q_k] u_{\lambda_i}(p_i) .
 \end{aligned} \tag{A.8}$$

Finally we see that $A_1^* = A_1$, $A_2^* = A_2$, as before, but $A_3^* = -A_3$; hence A_3 is purely imaginary and purely real at the same time. Thus A_3 must vanish if $J_\mu^{(p)}$ is to be both Hermitian and time reversal invariant.

All of this Dirac algebra would have been unnecessary had one known about current conservation, $\partial_\mu J_\mu^{(p)} = 0$. Indeed,

$$0 = \bar{u}_{\lambda_f}(p) [A_1 q_\mu \gamma_\mu + A_2 q_\mu P_\mu + i A_3 q^2] u_{\lambda_i}(p_i) \tag{A.9}$$

First, using the Dirac equation,

$$\bar{u}_{\lambda_f}(p_f) q_{\mu} \gamma_{\mu} u_{\lambda_i}(p_i) = \bar{u}_{\lambda_f}(p_f) [M_p - M_p] u_{\lambda_i}(p_i) = 0 .$$

Second,

$$\bar{u}_{\lambda_f}(p_f) q_{\mu} P_{\mu} u_{\lambda_i}(p_i) = \bar{u}_{\lambda_f}(p_f) [M_p^2 - M_p^2] u_{\lambda_i}(p_i) = 0 .$$

This leaves

$$0 = \bar{u}_{\lambda_f}(p_f) [i A_3(q^2) q^2] u_{\lambda_i}(p_i) . \quad (\text{A.10})$$

Hence $A_3(q^2) = 0$ for all $q^2 \neq 0$, and one can show that $A_3(0) = 0$ also.²

This completes the lengthy proof that current-conservation causes any time-reversal violating form factor to vanish as long as the proton remains on its mass shell (elastic scattering).

REFERENCES

1. S. D. Drell and M. A. Ruderman, Phys. Rev. 106, 561 (1957);
S. D. Drell and S. Fubini, Phys. Rev. 113, 741 (1959);
N. R. Werthamer and M. A. Ruderman, Phys. Rev. 123, 1005 (1961);
D. Flamm and W. Kummer, Nuovo Cimento 28, 33 (1963);
S. D. Drell and J. D. Sullivan, Phys. Letters 19, 516 (1965);
M. Gourdin, Diffusion des électrons de haute énergie (Masson et Cie, Paris, 1966);
G. K. Greenhut, Phys. Rev. 184, 1860 (1969).
2. M. N. Rosenbluth, Phys. Rev. 79, 615 (1950);
S. D. Drell and F. Zachariasen, Electromagnetic Structure of Nucleons (Oxford University Press, London, 1961).
3. T. Janssens et al., Phys. Rev. 142, 922 (1966);
H. J. Behrend et al., Nuovo Cimento 48, 140 (1967).
4. J. Mar et al., Phys. Rev. Letters 21, 482 (1968).
5. Y. S. Tsai, Phys. Rev. 122, 1898 (1961).
6. T. Powell, et al., Phys. Rev. Letters 24, 753 (1970).
7. L. Wolfenstein and J. Ashkin, Phys. Rev. 85, 947 (1952).
R. H. Dalitz, Proc. Phys. Soc. (London) A65, 175 (1952).
L. Wolfenstein, Ann. Rev. Nucl. Sci. 6, 43 (1956).
P. D. Grannis, Measurement of the Polarization Parameter in Proton-Proton Scattering from 1.7 to 6.1 BeV (Ph.D. thesis), UCRL-16070, August 1965.
8. M. Jacob and G. C. Wick, Ann. Phys. (N.Y.) 7, 404 (1959).
M. L. Goldberger, M. T. Grisaru, S. W. MacDowell, and D. Y. Wong, Phys. Rev. 120, 2250 (1960).

- P. D. Grannis, op. cit.
9. J. D. Bjorken and S. D. Drell, Relativistic Quantum Mechanics (McGraw Hill, New York 1964).
10. A. R. Edmonds, Angular Momentum in Quantum Mechanics, (Princeton University Press, Princeton, N. J. (1961).
11. S. M. Blenkii, L. I. Lapidus, R. M. Ryndin, Sov. Phys. Uspekhi, 7, 721 (1965); L. Wolfenstein, Ann. Rev. Nucl. Sci., op. cit.;
P. D. Grannis, op. cit.
12. The normal to the scattering plane for the following measurements is defined as in Eq. (2), except that \vec{p}_{in} is the momentum of the incident electron and \vec{p}_{out} is the momentum of the recoil proton:
Frascati: G. V. DiGiorgio et al., Nuovo Cimento 39, 471 (1965);
Orsay: J. C. Bizot et al., Phys. Rev. 140, B1387 (1965);
Stanford I: D. E. Lundquist et al., Phys. Rev. 168, 1547 (1968);
Stanford II: Dr. B. H. Wiik communicated to us a value of
$$P = (-0.006 \pm 0.020) \text{ measured at } q^2 = 0.27 \text{ (GeV/c)}^2$$
which was referred to in the paper by R. Prepost,
R. M. Simonds and B. H. Wiik, Phys. Rev. Letters 21, 1271 (1968).
13. Proceedings of the 1967 International Symposium on Electron and Photon Interactions at High Energies, Clearing house for Federal, Scientific, and Technical Information, N.B.S., U.S. Dep't of Commerce, Springfield, Va. UC-34-Physics (TID-4500, 51st edition);
Proceedings of the 1969 International Symposium on Electron and Photon Interactions at High Energies, Daresbury Nuclear Physics Laboratory, Daresbury, Nr. Warrington, Lancashire.

14. Drell and Zachariasen, Op. cit. (ref. 2)
15. In the literature one most often finds calculations and measurements of the ELECTRIC and MAGNETIC form factors, G_E and G_M respectively. G_E and G_M are linear combinations of F_1 and F_2 namely,
$$G_E = F_1 + \frac{q^2}{4M_p^2} F_2 \quad \text{while} \quad G_M = F_1 + F_2 .$$
16. J. D. Bjorken, Ph.D. thesis, (unpublished) Stanford Univ., Stanford, Calif. (1959); M. Gourdin and A. Martin, CERN Report 4804 (1962); T. A. Griffy and L. I. Schiff, "Electromagnetic Form Factors of Nucleons," found in High Energy Physics, Vol. I., E. H. S. Burhop ed., Academic Press, N. Y. (196); M. Gourdin, (ref. 1) op. cit.; R. Wilson (ref. 18) in Scottish Univ. Summer School (1966).
17. J. Bernstein, G. Feinberg, and T. D. Lee, Phys. Rev. 139, B1650 (1965).
18. L. N. Hand and Richard Wilson, SLAC Summer Study Report, SLAC 25-II, (1963) (unpublished); Richard Wilson, "Some Features of Electromagnetic Interactions" in Particle Interactions at High Energies, Scottish Universities' Summer School 1966, ed. T. Preist and L. Vick.
19. Drell and Zachariasen, op. cit., (ref. 2) pp. 15-18;
S. D. Drell, "Form Factors of Elementary Particles," in Proceedings of the International School of Physics, "Enrico Fermi", Course XXVI, "Selected Topics in Elementary Particle Physics". p. 205-208.
20. F. Guérin and C. A. Piketty, Nuovo Cimento 32, 971 (1964);
G. K. Greenhut, Ph.D. Thesis, Cornell University (1968)(unpublished);
J. Arafune and Y. Shimizu, Phys. Rev. 179, 1394 (1969);
(1970) 139 (1969).

21. A. Akhiezer, L. Rozentsveig, I. Shmushkevich, Sov. Phys. JETP, 6, 588 (1958).
22. N. Dombey, Rev. Mod. Phys. 41, 236 (1969);
N. Dombey, Phys. Letters, 29B, 588 (1969).
23. S. Rock, et al., Phys. Rev. Letters 24, 748 (1970).
24. R. B. Neal, ed. The Stanford Two-Mile Accelerator, W. A. Benjamin, Inc., New York (1968).
25. R. S. Larsen and D. Horelick, Report No. SLAC-PUB-398, Stanford Linear Accelerator Center (1968). (unpublished)
26. G. E. Fischer and Y. Murata, Report No. SLAC-PUB-605, Stanford Linear Accelerator Center (1969), (to be published in Nucl. Instr. and Methods). D. Yount, Nucl. Instr. Methods 52, (1-14)(1967).
27. Luke Mo, Stanford Linear Accelerator Center, SLAC-TN-65-40 (1965). (unpublished)
28. Gilbert Shapiro, Progr. in Nucl. Techn. and Instrumentation 1, 173 (1964);
C. D. Jeffries, Dynamic Nuclear Orientation, (Interscience Publishers, New York, 1963);
M. Borghini, CERN 68-32 NP (unpublished);
Proceedings of the International Conference on Polarized Targets and Ion Sources, Gif-sur-Yvette, France (1967) esp. the invited talk of O. Chamberlain which also appears as UCRL-17433 (unpublished).
M. Borghini, Ecole Internationale de la Physique des Particules Elementaires, Herceg Novi, Yugoslavia (1968).
29. M. Borghini, et al., Polarized Proton Target for Use in Intense Electron and Photon Beams, Nucl. Instr. and Methods 84, 168 (1970).

30. P. Roubreau, Ph.D. thesis, Grenoble 1966.
31. F. Seitz, Modern Theory of Solids (McGraw-Hill, N. Y. 1940) p. 191;
J. Clement and E. Quinell, Rev. Sci. Instr. 23, 213 (1952).
32. "Lektromesh" 100 x 100 holes per inch, 0.0015 inch thick, 35% open area, C. O. Jelliff Co., Southport, Conn.
33. W. N. Hardy and G. Shapiro, Proceedings of the International Conference on Polarized Targets and Ion Sources, Gif-sur-Yvette, France (1967).
34. V. K. Ermolaev, Yu N. Molin and N. Ya Buben, Kinetika i Kataliz 3, 58 (1962), English translation Kinetics and Catalysis 3, 46 (1962).
35. Fluorinated Ethylene Propylene film, type A, 0.0005 inch thick, Fluorocarbon Corp., Pine Brook, New Jersey.
36. C. H. Schultz, Scattering of 250 MeV positive Pi Mesons from a Polarized Proton Target (Ph.D. thesis), UCRL-11149, Jan. 1964.
C. D. Jeffries, op cit.
37. E. Fermi, Nuclear Physics, Rev. ed., p. 159, ed. J. Orear, A. Rosenfeld, R. Schluter (Univ. of Chicago, 1950).
38. C. C. Morehouse, et al., "Asymmetry in π^+ photoproduction from a polarized proton target at 5 and 16 GeV," (to be published).
39. P. D. Grannis, op. cit.
C. H. Johnson, Measurement of the Polarization Parameter in π^+ p Scattering from 750 to 3750 MeV/c (Ph.D. thesis), UCRL-17683, August 1967.

40. Charles C. Morehouse, private communication, work of reference 38, and Ph.D. Thesis (UCRL-19897) cited.
41. See e.g. N. Meister and D. Yennie, Phys. Rev. 130, 1210 (1963).
42. Robert N. Cahn and Y. S. Tsai, LRL, Berkeley, and SLAC SLAC-PUB-722 (April 1970) and submitted to Phys. Rev.
43. L. Camilleri, et al., Phys. Rev. Letters 23, 149 (1969).
44. F. J. Ernst, R. G. Sachs, K. C. Wali, Phys. Rev. 119, 1105 (1960).

LEGAL NOTICE

This report was prepared as an account of Government sponsored work. Neither the United States, nor the Commission, nor any person acting on behalf of the Commission:

- A. Makes any warranty or representation, expressed or implied, with respect to the accuracy, completeness, or usefulness of the information contained in this report, or that the use of any information, apparatus, method, or process disclosed in this report may not infringe privately owned rights; or*
- B. Assumes any liabilities with respect to the use of, or for damages resulting from the use of any information, apparatus, method, or process disclosed in this report.*

As used in the above, "person acting on behalf of the Commission" includes any employee or contractor of the Commission, or employee of such contractor, to the extent that such employee or contractor of the Commission, or employee of such contractor prepares, disseminates, or provides access to, any information pursuant to his employment or contract with the Commission, or his employment with such contractor.

TECHNICAL INFORMATION DIVISION
LAWRENCE RADIATION LABORATORY
UNIVERSITY OF CALIFORNIA
BERKELEY, CALIFORNIA 94720